Drug Resistance Updates 77 (2024) 101138

Contents lists available at ScienceDirect

Drug Resistance Updates

journal homepage: www.elsevier.com/locate/drup

Ultrastructural, metabolic and genetic characteristics of determinants facilitating the acquisition of macrolide resistance by *Streptococcus pneumoniae*

Xueqing Wu [a,b,1], Babek Alibayov [h,1], Xi Xiang [c], Santiago M. Lattar [e,2], Fuminori Sakai [e,2], Austin A. Medders [g], Brenda S. Antezana [d,f], Lance E. Keller [g,h], Ana G.J. Vidal [g], Yih-Ling Tzeng [d,f], D. Ashley Robinson [g,h], David S. Stephens [d,f], Yunsong Yu [a,b,*], Jorge E. Vidal [g,h,**]

[a] Department of Infectious Diseases, Regional Medical Center for National Institute of Respiratory Diseases, Sir Run Run Shaw Hospital, School of Medicine, Zhejiang University, Hangzhou 310052, China
[b] Key Laboratory of Microbial Technology and Bioinformatics of Zhejiang Province, Hangzhou 310052, China
[c] Department of Clinical Laboratory, Affiliated Jinhua Hospital, Zhejiang University School of Medicine, Jinhua 321000, China
[d] Department of Medicine, School of Medicine, Emory University, Atlanta, GA 30322, United States
[e] Hubert Department of Global Health, Rollins School of Public Health, Emory University, Atlanta, GA 30322, United States
[f] Graduate Program in Microbiology and Molecular Genetics, Emory University, Atlanta, GA 30322, United States
[g] Department of Cell and Molecular Biology, University of Mississippi Medical Center, Jackson, MS 39216, United States
[h] Center for Immunology and Microbial Research, University of Mississippi Medical Center, Jackson, MS 39216, United States

A B S T R A C T

Aims: To investigate the molecular events associated with acquiring macrolide resistance genes [*mefE/mel* (Mega) or *ermB*] in *Streptococcus pneumoniae* (*Spn*) during nasopharyngeal colonization.
Methods and results: Genomic analysis of 128 macrolide-resistant *Spn* isolates revealed recombination events in genes of the conjugation apparatus, or the competence system, in strains carrying Tn*916*-related elements. Studies using confocal and electron microscopy demonstrated that during the transfer of Tn*916*-related elements in nasopharyngeal cell biofilms, pneumococcal strains formed clusters facilitating their acquisition of resistance determinants at a high recombination frequency (rF). Remarkably, these aggregates comprise both encapsulated and nonencapsulated pneumococci that span extracellular and intracellular compartments. rF assessments showed similar rates regardless Mega was associated with large integrative and conjugative elements (ICEs) (>23 kb) or not (~5.4 kb). The rF for Mega Class IV(c) insertion region (~53 kb) was three orders of magnitude higher than the transformation of the capsule locus. Metabolomics studies of the microenvironment created by colonization of human nasopharyngeal cells revealed a link between the acquisition of ICEs and the pathways involving nicotinic acid and sucrose.
Conclusions: Pneumococcal clusters, both extracellular and intracellular, facilitate macrolide resistance acquisition, and ICEs were acquired at a higher frequency than the capsule locus. Metabolic changes could serve as intervention targets.

1. Introduction

Streptococcus pneumoniae (*Spn*), a Gram-positive opportunistic pathogen, is a leading cause of community-acquired pneumonia, meningitis, and otitis media (Rodgers and Klugman, 2011; Weiser, 2010). The treatment for pneumococcal disease has been challenged in recent years due to the rise of antibiotic resistance, including resistance to macrolides and β-Lactams in pneumococcal strains (Malisova et al., 2019; Aliberti et al., 2019; Kim et al., 2016).

In addition to causing diseases, *Spn* also asymptomatically colonizes in the nasopharynx, forming biofilms (i.e., bacteria aggregates) and shares this niche with several other streptococci and non-streptococci

* Corresponding author at: Department of Infectious Diseases, Regional Medical Center for National Institute of Respiratory Diseases, Sir Run Run Shaw Hospital, School of Medicine, Zhejiang University, Hangzhou 310052, China.
** Corresponding author at: Department of Cell and Molecular Biology, University of Mississippi Medical Center, Jackson, MS 39216, United States.
E-mail addresses: yvys119@zju.edu.cn (Y. Yu), jvidal@umc.edu (J.E. Vidal).
[1] Author contributed equally to this work.
[2] Current affiliation: FS: Pfizer Japan Inc., Tokyo Japan. SL: Department of Microbiology, Institute of Biological Science, Federal University of Minas Gerais, Belo Horizonte, BH, Brazil.

https://doi.org/10.1016/j.drup.2024.101138
Received 15 February 2024; Received in revised form 13 August 2024; Accepted 13 August 2024
Available online 16 August 2024

species (Hall-Stoodley et al., 2008; Gilley and Orihuela, 2014; Chao et al., 2014; Shak et al., 2013; Simell et al., 2012). We and others have demonstrated that pneumococcal strains form biofilm consortia on abiotic surfaces as well as on human nasopharyngeal cells (Lattar et al., 2018; Vidal et al., 2011, 2013; Wu et al., 2017). Furthermore, human nasopharyngeal cells, cultivated in a bioreactor system, facilitated the swift acquisition of antibiotic resistance genes between two *Spn* strains with a high recombination frequency (rF) (Lattar et al., 2018; Antezana et al., 2023; Vidal et al., 2022).

Macrolide resistance in *Spn* is mainly attributed to modification of the macrolide target in the bacterial ribosome and to active efflux (Kim et al., 2016). The most common mechanism altering the bacterial ribosome target involves the methylation of the 23S rRNA by methyltransferases encoded by *ermB* and rarely by *ermTR* (Leclercq and Courvalin, 2002). Another mechanism conferring macrolide resistance to *Spn* strains is the two-component macrolide efflux genetic assembly (Mega) efflux pump (Gay and Stephens, 2001). Mega is encoded by a 5.5 kb, or 5.4 kb, element carrying the *mef(E)* and *mel* (listed also as *msrD*) operon (Gay and Stephens, 2001; Schroeder et al., 2019). *Spn* strains carrying Mega are resistant to 14- and 15-membered macrolides, but they are susceptible to lincosamides and streptogramin B, known as the M phenotype (Del Grosso et al., 2006).

The *mef(E)/mel* and/or *ermB* genes are often carried in integrative and conjugative elements (ICEs) of the Tn*916*-related family and Tn*5253*-related family, which also carry the *tetM* gene for resistance to tetracycline (Del Grosso et al., 2009; Chancey et al., 2015; Santoro et al., 2014). The Tn*916*-related elements carrying Mega inserted into *orf6* are termed Tn*2009* (Chancey et al., 2015; Del Grosso et al., 2004). Tn*916*-related elements were identified in macrolide-resistant *Spn* strains isolated in the late 1960s (Wyres et al., 2013) but their prevalence has significantly increased in the last few years. Invasive and nasopharyngeal *Spn* strains carrying Tn*916*-related ICEs, including Tn*2009,* Tn*2010* and Tn*6002* and other ICEs, have been identified in China, Italy, Venezuela, USA, Spain, and the UK (Chancey et al., 2015; Santoro et al., 2014; Nikolaou et al., 2020; Domenech et al., 2014). Moreover, ~90 % of emergent *Spn* vaccine escape strains of serotype 35B and 35D, isolated in Japan, carry macrolide and tetracycline resistance determinants in Tn*916*-related ICEs; of these 75 % *Spn* strains carried Mega in Tn*2009 (*Shinohara et al., 2023*)*. Vaccine escape serotype 3 strains clonal complex (CC180) clade II, isolated in the USA and Hong Kong, carry *ermB* and *tetM* in a 36.7 kb Tn*916*-related ICE (Azarian et al., 2018).

In other Gram-positive species, the transfer of Tn*916*-related elements relies on the conjugation machinery (i.e., a type IV secretion system, T4SS), encoded in these ICEs (Johnson and Grossman, 2015). The molecular mechanism by which ICEs are acquired by *Spn* strains has been debated for over 25 years. However, the most common hypothesis suggests that acquisition occurs via transformation (Del Grosso et al., 2006; Chancey et al., 2015; Del Grosso et al., 2004). This hypothesis was based on the observation that conjugative insertion of Tn*2009* or Tn*2010* in *Spn* strains were infrequent (Chancey et al., 2015; Santoro et al., 2014), that *in vitro* conjugation assays have been unsuccessful to generate transconjugants (Del Grosso et al., 2006, 2004) or that the conjugative transfer of Tn*916* or Tn*916*-related ICEs, when it has been observed, occurred at a low ($<10^{-6}$) conjugation frequency (Watson and Musher, 1990), i.e., relative to the transformation frequency that can be as high as $<10^{-3}$. In recent years, we developed an *ex-vivo* human nasopharyngeal cell bioreactor system that facilitates the natural transference of mutation-mediated resistance (Lattar et al., 2018), as well as macrolide resistance carried in ICEs among *Spn* strains (Antezana et al., 2023; Vidal et al., 2022). Using the bioreactor system, we demonstrated that the transformation machinery, specifically the Com system, facilitates the acquisition of Mega, carried in Tn*916*-related elements, at a recombination frequency (rF) as high as 10^{-3}. In the absence of either a functional Com system or a functional transformation apparatus, the rF of the acquisition of Tn*916*-related ICEs fell to $<10^{-7}$ (Antezana et al., 2023).

Competence development is a physiological state that is tightly regulated by environmental cues and cellular determinants. Although the acquisition of antibiotic resistance naturally occurs when *Spn* strains colonize the human host (Chaguza et al., 2020), the human cell determinants are largely unknown. These host cell-derived molecules are mimicked in the bioreactor system, as pneumococci become naturally competent, release extracellular DNA and acquire DNA at a high rF (Lattar et al., 2018; Antezana et al., 2023). This occurs in the absence of antibiotic selective pressure, and within a few hours of incubation. At present, important molecular events, human cellular factors, and the ultrastructural dynamics of ICE transfer among *Spn* strains have remained unexplored.

In a recent study, we isolated and whole genome sequenced *Spn* strains from pneumococcal disease cases in China (Wu et al., 2022; Lan et al., 2023). The prevalence of macrolide resistance in these *Spn* strains was 100 % (N=128). In the current study, we conducted a genomic analysis of genetic elements conferring macrolide resistance in these strains and identified potential hotspots and other genetic characteristics that are linked to the acquisition of macrolide resistance. Subsequently, we performed a detailed investigation of human nasopharyngeal biofilms, and cellular, and metabolic determinants leading to the acquisition of macrolide resistance.

2. Results

2.1. Identification of macrolide resistance determinants and recombination in erythromycin-resistant pneumococcal strains

To identify the genetic determinants of macrolide resistance, we performed whole-genome sequence analysis on 128 clinical isolates that were resistant to erythromycin (Wu et al., 2022). These isolates belonged to 20 different serotypes (S) (Fig. 1A). S19F strains were most prevalent (n=43), followed by S19A strains (n=16). Our genomic analysis revealed that all macrolide resistance determinants were found in *Tn916*-related elements. The majority of S19F and S19A strains carried Mega and *ermB* in Tn*2010* elements, and were phylogenetically classified in clonal complex (CC) 271 (Croucher et al., 2014) (Fig. 1A). Other stains carried only *ermB* which was located in Tn*6002* elements. We identified one strain carrying *ermB* in Tn*3782* (Fig. 1A).

We then performed an analysis on recombination events within the Tn*916*-related elements. Because the transformation machinery facilitates acquisition of Tn*916*-related elements (Antezana et al., 2023), we analyzed the genomic region carrying genes of the competence locus *comCDE* (Claverys et al., 2009). The most common recombination hotspots, within the Tn*2010* elements, were located in genes encoding a putative type 4 secretion system [T4SS, (i.e., the conjugation apparatus)] and *ermB*, which is inserted within *orf20* (Fig. 1B). Recombination events downstream of the T4SS genes were not identified in these *Spn* CC271 strains (Fig. 1B). Recombination hotspots in the locus *comCDE*, were only identified in S14 and S23F strains (Fig. 1C). These strains carry Tn*6002* elements (Fig. 1A) but hotspots were not identified in their ICEs (not shown). In most other strains, genes encoding the Com system were conserved with no evidence of recombination (Fig. 1C). Collectively, strains harboring Tn*916*-related elements were observed to possess recombination hotspots either within the genes encoding the conjugative machinery of Tn*2010* or within the locus that regulates pneumococcal competence for DNA uptake but not in both.

2.2. Spatial localization of pneumococcal strains within nasopharyngeal biofilm consortia

We next investigated the mechanisms behind the acquisition of macrolide resistance genes. Fitness, colonization dynamics, and ultrastructure of various pneumococcal strains, including strains carrying Tn*916*-related elements, were studied during co-colonization in the *ex-*

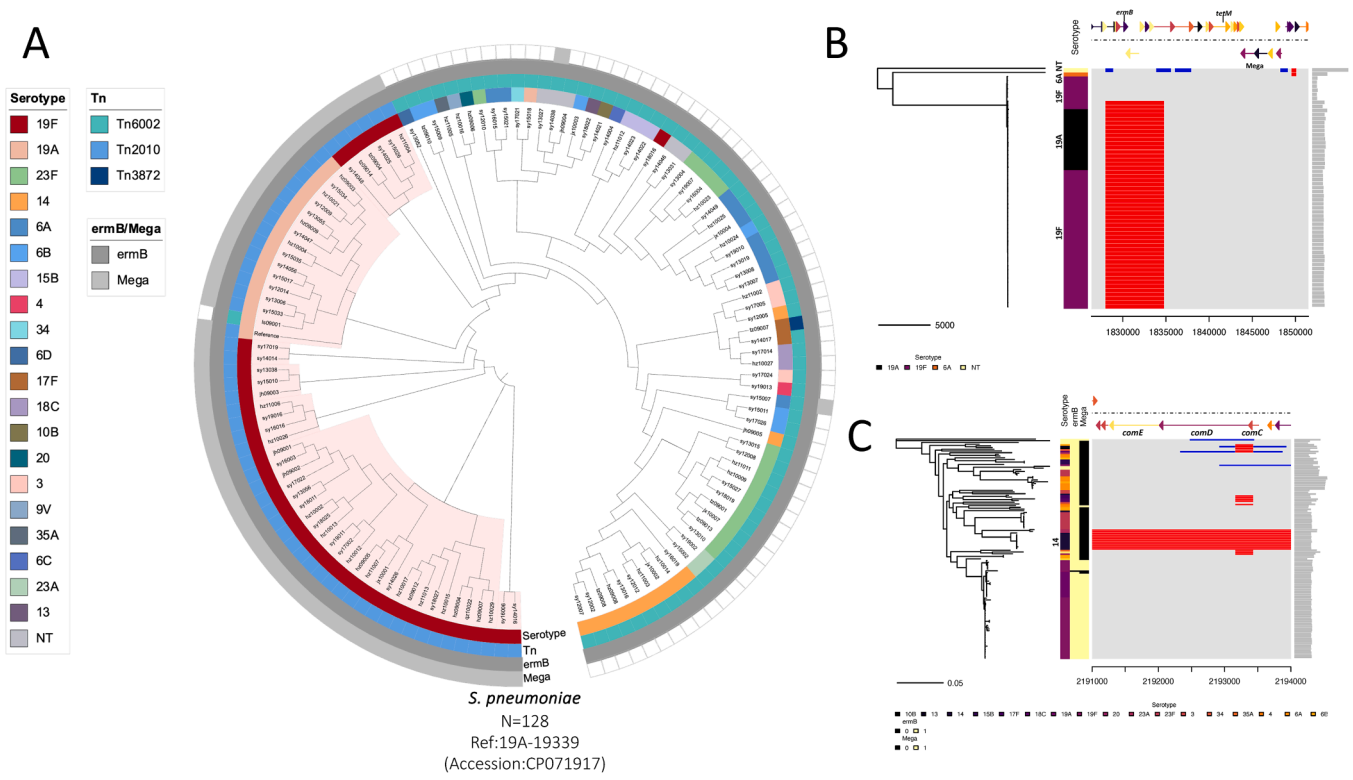

Fig. 1. The phylogenetic tree and recombination events in macrolide-resistant clinical pneumococcal isolates. Phylogenetic tree of macrolide-resistant pneumococcal isolates (N=128, Accession: PRJNA795524) that constructed in FastTree (http://www.microbesonline.org/fasttree/) using SNP calling data from Snippy (https://github.com/tseemann/snippy) (A). The metadata of serotype (different color strips), the presence of the *ermB* gene (dark grey circle), the presence of the Mega element (light grey: positive; blank space: negative), and the Tn type for each of the pneumococcal isolates were marked at the tip of the tree. The branches (serotypes 19 F and 19 A) with light red shades emphasize strains carrying the Mega element. (B). The visualized recombination prediction in the region of *Tn916*-like using the strains carrying Mega element (n=58) that were mapped against an annotated chromosome of the reference pneumococcal strain 19A-19339 (Accession: CP071917) using Snippy and Gubbins (https://github.com/nickjcroucher/gubbins). Red blocks represent the recombination blocks in each clone complex on an internal branch, which are shared by multiple isolates, while blue blocks represent the recombination occurred on terminal branches, which are unique to individual isolates. The whole data set was visualized with RCandy (https://github.com/ChrispinChaguza/RCandy) in RStudio (Version 2023.09.1+494). The serotype data was aligned with each strain where most strains carrying Mega belong to serotypes 19 A and 19 F. The recombination events were detected at the *ermB* gene region. One NT strain was detected to have new recombination regions (blue blocks) not include the *ermB* gene. No recombination event was detected in the Mega region. (C) Recombination prediction for *comCDE* region using all strains and the same methods as described above for panel (B), where the recombination was only observed in strains that do not carry Mega, especially for serotype 14 strains.

vivo bioreactor system (Lattar et al., 2018). Mixtures of pneumococcal strains were inoculated in the bioreactor including reference strain TIGR4, and *Spn* strain 8655 that carry the macrolide resistance gene *ermB* in a Tn*3872*-element (8655^{Tn3872}) (Wu et al., 2017; McDougal et al., 1998), or TIGR4 and strain D39. The growth rates of TIGR4 and 8655^{Tn3872}, or TIGR4 and D39, when inoculated separately in Todd-Hewitt broth with yeast extract (THY) were similar (not shown). When strains co-colonized the simulated human pharyngeal epithelium, the density of 8655^{Tn3872} biofilms (~10^8 cfu/ml) was significantly higher than that of TIGR4 (~10^7 cfu/ml) (Fig. 2A) while the density of TIGR4 when co-inoculated with D39 was similar (Fig. 3A).

We tested the hypothesis that the two pneumococcal strains will be in physical proximity to enhance the efficiency of gene transfer while forming a biofilm consortium. To visualize individual strains within the biofilm consortium, we stained pneumococci with fluorescence-labeled serotype-specific antibodies, and the DNA with DAPI. Preparations were analyzed with both a confocal microscope and a super-resolution confocal microscope. Biofilm consortium formed by a mixture of TIGR4 and 8655^{Tn3872} (Fig. 2C) or TIGR4 and D39 (Fig. 3B) were attached to human pharyngeal cells forming bacterial aggregates. Surprisingly, structural confocal analysis of the XY plane, XZ and XY optical sections, showed intracellular TIGR4 and 8655^{Tn3872} pneumococci (Fig. 2C). Optical XY sections, each spaced 0.1 μm apart from the top and bottom of the projection, revealed that the TIGR4 and 8655^{Tn3872} aggregate locates on top but enters pharyngeal cells and these pneumococci are positioned on the same focal plane as that of cell nuclei (Fig. 2C). Remarkably, intracellular pneumococci consisted of both encapsulated and nonencapsulated bacteria (Fig. 2C, arrow). Quantification of the median fluorescence intensity, from each channel, was significantly higher for 8655^{Tn3872} compared with TIGR4 (Fig. 2B). Consistent with the increased density of 8655^{Tn3872}. The median area of the largest bacterial aggregates of 8655^{Tn3872} was 1684 μm (Weiser, 2010) while that of TIGR4 was 155 μm (Weiser, 2010) (not shown).

Super-resolution microscopy (Fig. 2D) and colocalization analysis shown in Fig. 3B (arrows) identified physical contact between pneumococci within biofilm consortia. Physical contact spanned over ~1.2 μm of capsule-capsule interaction (Fig. 2D, dotted line) with 3D analysis showing the embedding of both capsules (Fig. 2D, arrow).

2.3. *Pneumococci form localized aggregates on pharyngeal cells*

Ultrastructural studies using scanning electron microscopy (SEM) and transmission electron microscopy (TEM) confirmed findings on confocal microscopy. These studies showed that pneumococci by the time of transformation had occurred in the bioreactor (Lattar et al., 2018) (i.e., 6 h post-inoculation, explained in the next section), are organized in localized clusters of bacterial aggregates attached to pharyngeal cells (Fig. 3C, delimited). Pneumococci were also observed

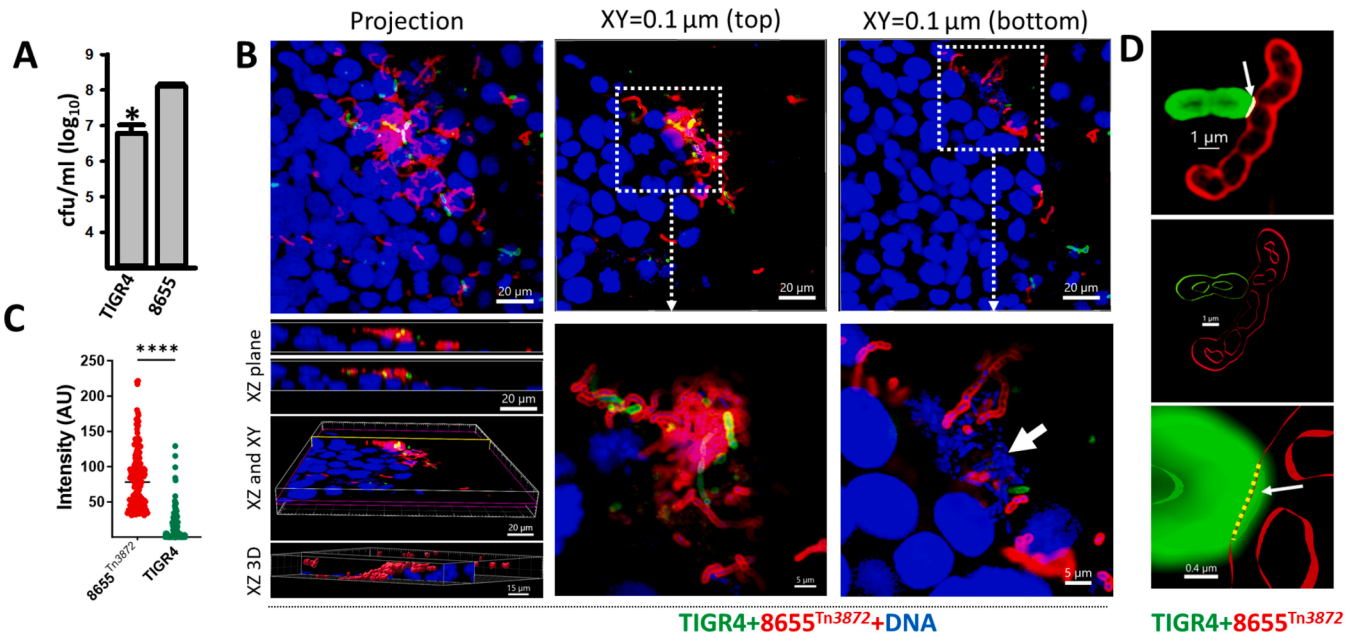

Fig. 2. Competitive dynamics of pneumococcal strains during acquisition of resistance. (A) *S. pneumoniae* strain TIGR4 (SPJV23), and strain 8655^{Tn3872} (S6B) were co-inoculated into a bioreactor with human pharyngeal cells, and incubated for 6 h after which biofilms were collected, serially diluted, and plated onto different BAP with specific antibiotics. The error bars represent the standard error of the means calculated using data from at least three independent experiments. (B-C) Strains were stained with an anti-S4/A488 (green) and an anti-S6B/A555 (red) antibodies while the DNA was stained with DAPI (blue). Micrographs were obtained with a confocal microscope and analyzed with the Imaris software. (B) The fluorescence intensity in arbitrary units (AU) obtained from each channel was graphed. The error bars represent the standard error of the means calculated using data from two independent experiments. ****p <0.0001. (C) Confocal micrographs. Left panels: the projection, the XZ plane, both Z and XY planes, and XZ plane of a 3D reconstruction are shown. Middle panel and right panel: XY optical sections of 0.1 µm each sliced from the top and the bottom are shown. The delimited regions are magnified in the bottom panels. The arrow points out intracellular pneumococci. (D) Imaging analysis using the Imaris software analyzed micrographs obtained by super-resolution microscopy. Arrows point (top and bottom panel) out the area of physical colocalization.

inside the cells, evidenced by disrupted membrane structures observed at various magnifications, resembling holes (Figs. 3D and 3E, arrows). Under SEM, extracellular pneumococci within clusters appear elongated (Fig. 3F-3 H) and structures compatible with the type IV pili (T4P) were observed (Figs. 3F and 3H, white arrows). T4P were also evident in bacterial clusters observed in micrographs collected by TEM (Fig. 3I, arrows). Within each cluster, some pneumococcal cells were observed lysed, which was characterized by the presence of bacteria with a disrupted cell wall (Figs. 3F and 3H, black arrows). Each cluster of pneumococci was surrounded by pharyngeal cells that appeared damaged such as those detached from the substratum or with a compromised cell membrane (Fig. 3D-G, stars).

2.4. *Mega can be transferred in an ex vivo nasopharyngeal environment from disease isolates or engineered pneumococci*

We next investigated the frequency of Mega acquisition by a recipient *Spn*. To assess this, we inoculated in the *ex vivo* bioreactor model a pair of strains including a *Spn* strain isolated from pneumococcal disease carrying Mega in the chromosome, Mega-1.III (GA17570) or Mega-2.II (GA41688) (Schroeder et al., 2019), and a recipient D39 carrying resistance to tetracycline and streptomycin (D39$^{Str\text{-}Tet}$). The recombination frequency (rF) of D39$^{Str\text{-}Tet}$ to acquire Mega from GA17570, or from GA41688, was 2.44×10^{-7} or 1.18×10^{-5} respectively (Fig. 4A, and B). The colonization density (cfu/ml) of the recipient D39$^{Str\text{-}Tet}$ when co-inoculated with either donor strain was similar, thereby the differences cannot be attributed to a decreased population of the recipient (Figs. 4A and 4B, right panels). Tetracycline resistance was acquired by Mega-carrying strains (i.e., from D39$^{Str\text{-}Tet}$) at a rF of 7.59×10^{-5} (GA17545, Fig. 4A), or 8.15×10^{-5} (GA41688, Fig. 4B).

Whole genome sequencing confirmed that in strain D39$^{Mega/GA17570}$ the Mega element was in the same chromosome site as that in the donor GA17570 (Fig. 4C). The region is located between the capsular polysaccharide biosynthesis protein *capD* gene (SPD_0099/SPAR50_0099, D39/GA17570 nomenclature) and SPD_0101/SPAR50_108, a gene encoding for a putative hydrolase (Fig. 4C).

Since the rF to acquire Mega-1.III versus Mega-2.II was different, we investigated if the location of Mega in the chromosome influences the rF by assessing the transfer of Mega from strains with the same genetic background. To this purpose, TIGR4 strains were engineered to carry Mega class 1.I, 1.III, 2.II, or 2.IVc in the chromosome (Supplementary Table S1). A recipient D39$^{Str\text{-}Tet}$ was incubated in the bioreactor with a TIGR4^{Mega} strain and the rF was investigated. D39$^{Str\text{-}Tet}$ recombinants now carrying macrolide resistance in a Mega element (D39$^{Str\text{-}Tet/Mega}$) were obtained at a similar rF $>2.01\times10^{-3}$ (Fig. 4D). Using a qPCR approach, we confirmed that >94.5 % of D39$^{Str\text{-}Tet/Mega}$ recombinant strains carried capsules genes for serotype 2 (Fig. 4E). Acquisition of Mega by D39$^{Str\text{-}Tet}$ was inhibited by treatment with DNaseI indicating that this genetic element (≥5.4 kb) conferring macrolide resistance was acquired by transformation (Fig. 4D). Taken together, Mega can be transferred at a high frequency but the chromosomal region where Mega is located does not influence the transfer.

2.5. *Recombination frequency of the acquisition of Mega associated, or not associated, with integrative and conjugative elements*

We have demonstrated that acquisition of large ICEs by *Spn* occurs in the bioreactor and that acquisition is facilitated by the transformation machinery (Antezana et al., 2023; Vidal et al., 2022). We therefore sought to compare, under the same culture conditions of the bioreactor, the rF for the acquisition of macrolide resistance encoded in genetic elements of varying sizes (~1, ~5.5, ~23.5, or ~53 kb) associated or not with ICEs. To this end, we engineered, or selected, pneumococcal strains carrying macrolide resistance genes *ermB* (TIGR4$^{\Omega ermB}$) or *mef*

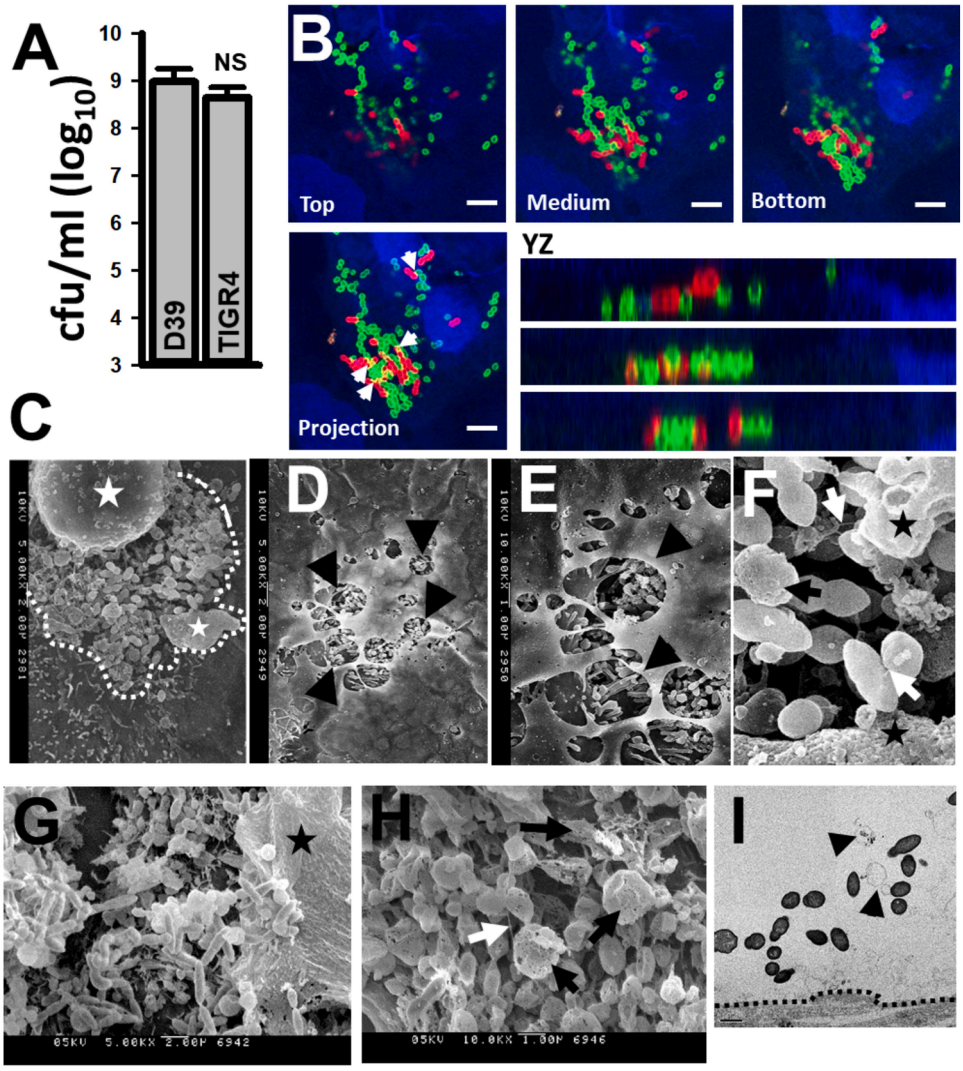

Fig. 3. Pneumococcal biofilm consortia on human pharyngeal cells. (A) *S. pneumoniae* TIGR4 (SPJV24) and D39 (SPJV22) derivatives were co-inoculated into a bioreactor with human pharyngeal cells, and incubated for 6 h after which biofilms consortia were harvested, serially diluted, and plated onto different BAP with specific antibiotics. The error bars represent the standard error of the means calculated using data from at least three independent experiments. (B) Pneumococcal strains were incubated as above and then biofilms were stained with an anti-S4/A488 (green), an anti-S2/A555 (red) antibodies and the DNA was stained with DAPI (blue). Bar=5 μm. Preparations were analyzed by confocal microscopy. xy optical sections from the top, middle, or bottom sections, the xy projection, and yz optical sections, are shown. (C-I) Strains were incubated as above in the bioreactor after which pneumococcal strains were fixed and submitted to SEM (C-H) or TEM (I) image acquisition. In (C-H) white dotted line=microcolony, arrowheads=intracellular pneumococci, stars=human pharyngeal cells, black arrows=lysed pneumococci, white arrows=nanotube-like structures connecting pneumococci. In (I) black dotted line=surface of epithelial cell, arrowheads=pili-like structures.

(E)/mel (i.e., Mega) either not associated to ICEs (TIGR4$^{Mega1.I}$ or TIGR4$^{Mega2.IVc}$) or carried it within Tn*2009* (GA16833) (Fig. 5A) or Mega Class IV(c) insertion (GA17545). Since Tn*2009* also carries the *tetM* gene for tetracycline resistance, we utilized a recipient strain D39 carrying mutations ~800 bp apart in the *rpsL* and *folA* gene, conferring resistance to streptomycin and trimethoprim (D39$^{Str\text{-}Tmp}$), respectively. Mutations and genes associated with resistance were confirmed in the recipient and donor strains by whole genome sequencing (Antezana et al., 2023).

The rF of recipient D39$^{Str\text{-}Tmp}$ acquiring macrolide resistance from the engineered TIGR4 donor strains and that carried either a ~1 kb (Ω*ermB*), ~5.4 (Mega1.I), or ~5.5 kb (Mega2.IVc) occurred at a similar rF with a median of 5.03×10^{-5} (Fig. 5B). The donor strain, TIGR4$^{\Omega ermB}$, TIGR4$^{Mega1.I}$ or TIGR4$^{Mega2.IVc}$ did not acquire streptomycin or trimethoprim resistance (not shown) from recipient D39$^{Str\text{-}Tmp}$ under the bioreactor incubation condition (Lattar et al., 2018).

Remarkably, the rF for the acquisition of Mega carried in Tn*2009* (~23.5 kb) or Mega2.IVc (~53 kb), from donor strain GA16833, or GA17545, respectively, was similar to rFs of the engineered TIGR4 strains, with a median rF of 5.47×10^{-5}, or rF=3.50×10^{-4}, respectively (Figs. 5C and 5D). Unlike TIGR4 that did not acquire resistance from the recipient strain, donor strains GA16833 (Tn*2009*) and GA17545 (Mega Class IV(c) insertion) acquired streptomycin resistance from D39$^{Str\text{-}Tmp}$ at a rF of 9.65×10^{-5} or 5.89×10^{-5}, respectively, thereby confirming the micro-environment of the bioreactor allowed for bidirectional exchange of DNA.

We then conducted PCR analysis to confirm that *ermB*, or the Mega element, was acquired by the recipient. PCR analysis of ten different transformants confirmed that in D39$^{\Omega ermB}$ the *ermB* gene was located downstream *dexB* in the same location as that of the donor strain TIGR4$^{\Omega ermB}$ but absent in the recipient D39$^{Str\text{-}Tmp}$ (Fig. 5E). For example, PCR using primers SL1-SL2 amplified a ~4.3 kb fragment in both TIGR4$^{\Omega ermB}$ and D39$^{\Omega ermB}$ but a ~2 kb fragment in D39$^{Str\text{-}Tmp}$ due to the absence of *ermB* and SP0343 (Figs. 5A and 5E). The Mega element, *mef (E)/mel,* was also amplified from ten D39$^{Mega1.I}$ transformants and PCR analysis located the insertion within the same site of the chromosome

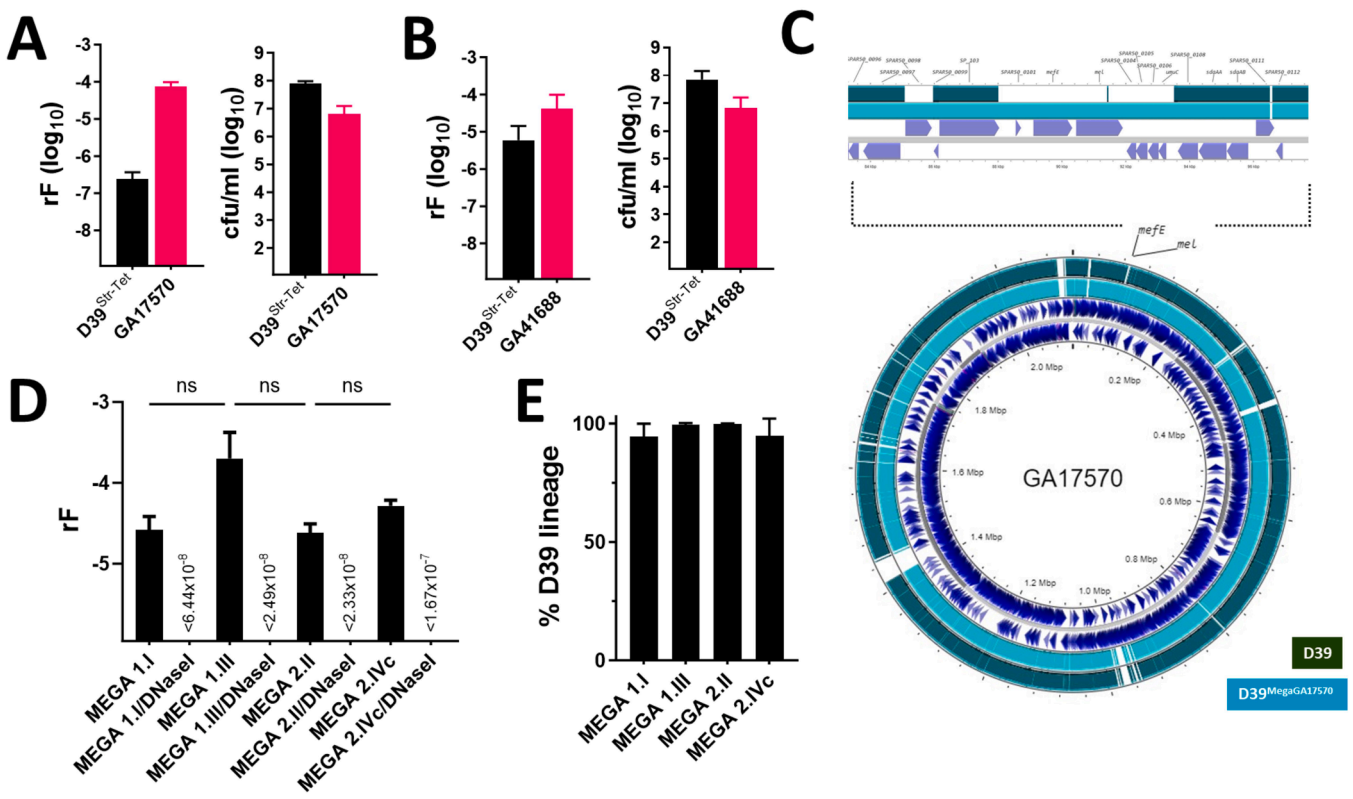

Fig. 4. Transference of macrolide resistance carried in Mega. (A) *S. pneumoniae* D39 (SPJV54) and GA17570, or (B) SPJV54 and GA41688 were co-inoculated into the bioreactor and incubated for 6 h after which biofilms were collected, serially diluted, and plated onto blood agar plates containing the appropriate antibiotic mixture. Each parent strain, or transformants from each lineage was counted. The recombination frequency (rF) was calculated (left panels) and density of each strain was shown (right panels). (C) Recipient strain D39 and transformant D39^{Mega17570} were mapped against donor strain GA17570. Insertion of Mega (*mefE/mel*) into D39^{Mega17570} and a fragment of at least ~9 kb from donor were shown. (D) D39 (SPJV22) was inoculated in the bioreactor along with TIGR4 carrying Mega 1.I, Mega 1.III, Mega 2.II, or Mega 2.IVc, and incubated for 6 h. In parallel experiments performed with each pair of strains, the culture medium was supplemented with DNase I. Biofilms were harvested and the rF was calculated as above. (E) SPJV22 recombinants (i.e., carrying Mega) were pooled, the DNA was extracted and used in serotype specific qPCR reactions to detect the total copies of serotype 2 (SPJV22) or serotype 4 (TIGR4-Mega derivative). The percentage of SPJV22 (D39 lineage) was used to construct the graph. In panels (A, B, D and E) the error bars represent the standard error of the means calculated using data from at least three independent experiments.

(not shown).

PCR reactions amplified similar PCR products using DNA from both GA16833 and D39^{Tn2009} that were absent when the DNA template was purified from D39$^{Str\text{-}Tmp}$ (Fig. 5F, listed as F2, F3, and F4). As expected, two PCR products (F5 and F6) were amplified using DNA from D39$^{Str\text{-}Tmp}$ but were absent in GA16833 and D39^{Tn2009} (Fig. 5F). These results revealed that the acquisition of macrolide resistance occurs at a similar frequency in strain D39 regardless Mega is associated, or not, with an ICE, and regardless of the molecular size of the ICE.

2.6. Microenvironment and metabolomic changes during pneumococcal ICE acquisition

Pneumococcal ICEs are transferred in the bioreactor with human pharyngeal cells at a high frequency (Antezana et al., 2023; Vidal et al., 2022). To gain further insight into the mechanism we analyzed the primary metabolism during the transfer of an ICE. We analyzed supernatants from bioreactors that had been left uninfected, infected with D39 and GA16833 (i.e., ICE acquisition by D39) or infected with D39Δ*comD* (SPJV31) and GA16833 (i.e., no acquisition). Supernatants were collected for 60 min, between 1 and 2 h post-inoculation (labeled as 2 h), or 3 and 4 h post-inoculation (labeled as 4 h). First, partial least squares discriminant analysis (PLSDA) was conducted to investigate if the groups were separable. After merging the two time points of each infection condition, the overall error rate using centroid distance demonstrated that metabolites in cells infected with D39 and GA16833 were more different than the other two groups (Fig. 6A). PLSDA further identified metabolites from pharyngeal cells incubated with D39 and GA16833 for 2 h as the most distinct (Fig. 6B).

When the relative abundance of the metabolites was assessed, the levels of nicotinic acid and sucrose were different in supernatants from cells infected with D39 and GA16833, or with D39Δ*comD* and GA16833, compared with the uninfected control (Fig. 6C and Supplementary Table S2). However, these metabolites were ~10-fold more down-regulated in bioreactor supernatant where the transfer of the ICE occurred (i.e., D39 and GA16833 compared with D39Δ*comD* and GA16833) (Fig. 6C and Supplementary Table S3). We conducted a comparison between the metabolites found in the supernatants from pharyngeal cells infected with D39 and GA16833 and those from cells infected with D39Δ*comD* and GA16833. Nine known molecules including nicotinic acid (~8-fold increase) and sucrose (~11-fold increase) were enriched in supernatants from human NP cells infected with D39Δ*comD* and GA16833.

Nicotinic acid (vitamin B3 or niacin) is a precursor of NAD (Nicotinamide Adenine Dinucleotide) and NADP, two molecules important for bacterial physiology. Since the role of nicotinic acid in the acquisition of resistance by *Spn* is unknown, we conducted a protein interaction network analysis using STRING. A conserved hypothetical protein with sequence homology to nicotinate phosphoribosyltransferase (Spr1277, R6 nomenclature) (French et al., 2010) that catalyzes the first step in the biosynthesis of NAD from nicotinic acid yielded 25 edges and 11 nodes in the STRING database. The proteins shown in Fig. 6D are biologically

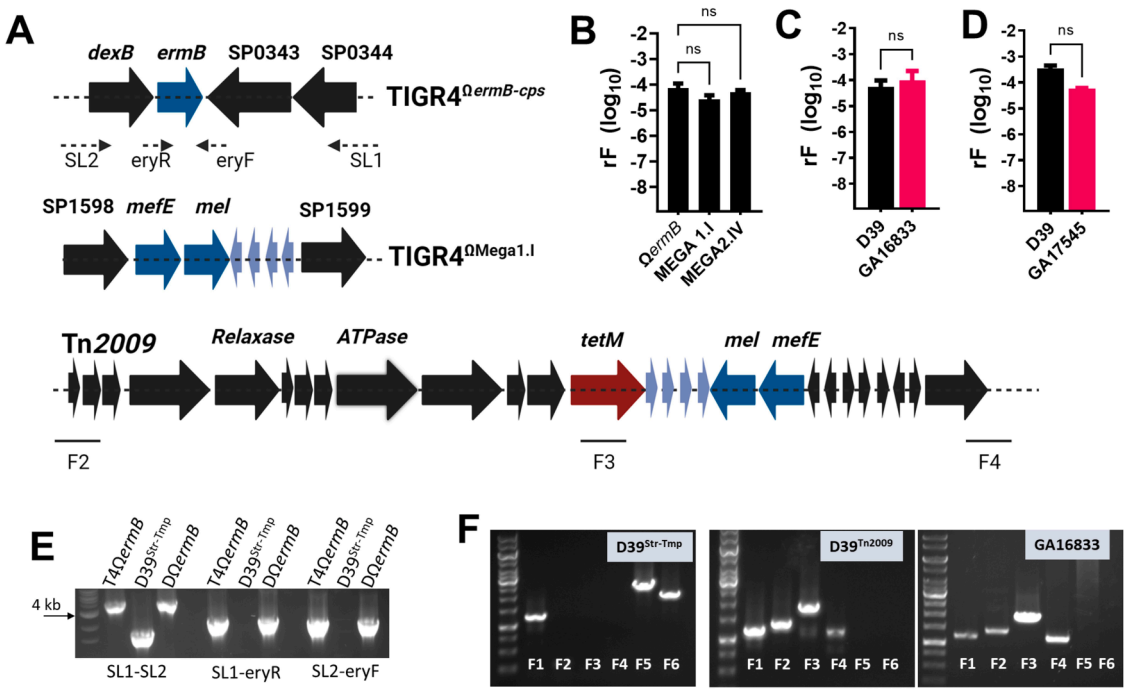

Fig. 5. Transference of macrolide and tetracycline resistance carrying transposon Tn2009. (A) Genomic context of the insertion of *ermB* in TIGR4$^{\Omega ermB}$, or Mega (*mefE/mel*) in TIGR4$^{\Omega Mega1.I}$. Primers SL2, eryR, eryF and SL1, underneath the top panel were utilized below. The map of Tn2009 from GA16833 is shown, indicating the location of genes encoding for the relaxase, and ATPase, of the putative type IV secretion apparatus, and genes *tetM*, *mefE* and *mel*. (B-D) D39 (SPJV33) was inoculated in the bioreactor along with (B) TIGR4$^{\Omega ermB}$, TIGR4$^{\Omega Mega1.I}$, or TIGR4$^{\Omega Mega2.IV}$ or (C) GA16833, or (D) GA17455. Experiments were incubated for 6 h and biofilm bacteria were harvested from the bioreactor, diluted and plated onto blood agar plates containing the appropriate antibiotics to investigate the recombination frequency (rF). The error bars represent the standard error of the means calculated using data from at least three independent experiments. NS=no significant. (E) DNA was purified from TIGR4$^{\Omega ermB}$ (T4Ω*ermB*), SPJV33 (D39$^{Str\text{-}Tmp}$) or SPJV33$^{\Omega ermB}$ (DΩ*ermB*) and used as template in PCR reactions with primer pairs SL1-SL2, SL1-eryR, or SL2-eryF. (F) DNA was purified from SPJV22 (D39$^{Str\text{-}Tmp}$), D39^{Tn2009}, or GA16833, and utilized as template in PCR reactions with pair of primers F1-F5.

connected. As expected, Spr1277 showed direct interaction with NAD biogenesis proteins such as NanC, NadD, NadE, and NadK. Besides these proteins, a direct STRING interaction was obtained with the competence induced protein A (CinA). No interactions were observed in STRNG when sucrose-6-phosphate hydrolase (ScrB), which enables bacteria to metabolize sucrose, was used to analyze the network against all other enzymes derived from the metabolomics analysis, i.e., Spr1277, NanC, or CinA. These results suggested that the acquisition of the pneumococcal ICE resulted in a significant alteration of metabolites involved in nucleic acid synthesis and carbohydrate metabolism.

2.7. Enhanced transformation frequency for the acquisition of Mega Class IV(c) insertion compared to acquisition of the capsule locus

The similar rF obtained in Fig. 5 experiments prompted us to further investigate if the entire ICE was acquired by most macrolide-resistant recombinants. Because the acquisition of pneumococcal transposons is facilitated by the transformation machinery (Antezana et al., 2023), we compared the rF of the large Mega Class IV(c) region which is adjacent to an ICE ~53 kb against that for the acquisition of the capsule *cps* locus (~23 kb), whose genes are acquired via transformation. To assess this, we took advantage that TIGR4$^{\Omega ermB}$ had been engineered to carry *ermB* ~5 kb upstream the first gene of the *cps* locus, *cps4A*. Given that there is high homology in the *cps* locus of the donor TIGR4$^{\Omega ermB}$ and the recipient strain D39, but the Mega Class IV(c) carries ~53 kb of heterologous DNA (Fig. 7A), we would have expected a higher rF for the acquisition of the *cps* locus compared with that of the acquisition of the full-length Mega Class IV(c) insertion region.

To identify transformants that had acquired the full-length Mega Class IV(c) insertion region (~53 kb), we first extracted DNA from D39$^{MegaIV(c)}$ transformants (N=100), and we performed eight PCR reactions with primers spanning the Mega Class IV(c) region (Fig. 7B). Fig. 7C shows representative PCR reactions of three different D39$^{MegaIV(c)}$ transformants either acquiring the full-length *region* (C1) or those that acquired Mega and short pieces of DNA downstream (C2) or only Mega (C3). Whole genome sequencing confirmed the acquisition of Mega Class IV(c) region by D39 (Fig. 7D). Notably, 54 % of D39$^{MegaIV(c)}$ transformants (54/100) acquired the ~53 kb *region* as investigated by the PCR approach. Having obtained the number of D39 $^{MegaIV(c)}$ transformants carrying full-length Mega Class IV(c), we re-calculated the rF to now reflect true acquisition of the entire Mega Class IV(c)/ICE region and the adjusted rF was $1.95x10^{-4}$ (Fig. 7E). There was, however, no statistical significance when we compared the rF for the acquisition of Mega (i.e., transformants growing on erythromycin plates) compared with that for acquiring the full-length Mega Class IV(c).

We preformed experiments in parallel with donor TIGR4$^{\Omega ermB}$ and recipient D39$^{Str\text{-}Tmp}$ and obtained a rF=$3.84x10^{-5}$ (Fig. 7F). Because the *cps* locus is highly similar between TIGR4 and D39 and conventional PCR mapping is not possible, we utilized qPCR assays that differentiate serotype 2 from serotype 4 (Pimenta et al., 2013), (Sakai et al., 2015) thereby D39$^{\Omega ermB}$ transformants with a *cps4* positive qPCR reaction represented D39 acquiring capsule genes from TIGR4. Only 12 % of these colonies (8/66) yielded a qPCR positive reaction for serotype 4. Conventional PCR using D39-specific primers (Fig. 7G) and wgs (Fig. 7D) confirmed that transformants were D39$^{\Omega ermB}$ that carried the *cps* from TIGR4 (i.e., D39$^{\Omega ermB\text{-}cps4}$). A mixture of anti-capsule antibodies against serotype 2 or serotype 4 capsule (anti-S2A555 and anti-S4A488) demonstrated that all eight D39$^{\Omega ermB\text{-}cps}$ expressed serotype 4 capsule whereas D39$^{\Omega ermB}$ strains with a negative PCR reaction for *cps4* expressed serotype 2 capsule (Fig. 7H). A mixture of donor and recipient showed that antibodies are specific for each capsular type (Fig. 7H). The adjusted rF for the acquisition of the *ermB-cps4* capsule locus (rF=$3.77x10^{-7}$) was significantly different to that of the acquisition of *ermB* (rF=$3.84x10^{-5}$) (Fig. 7F). We then deleted the *comCDE* locus in

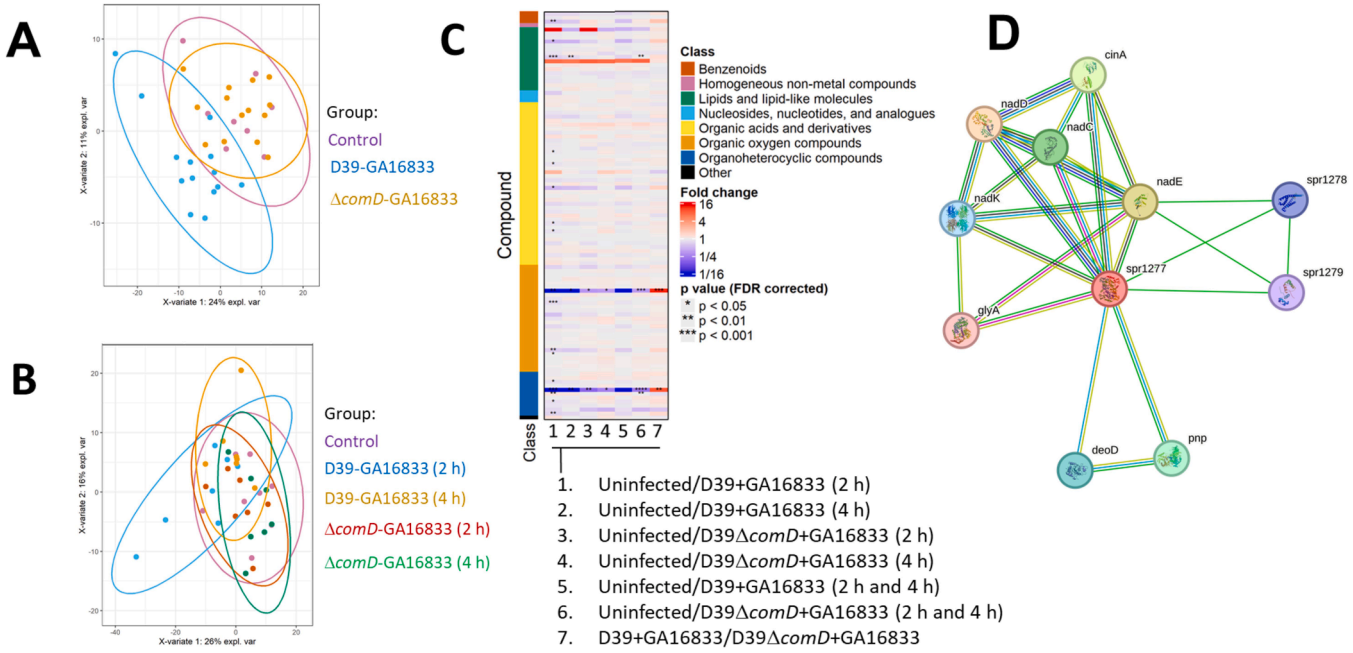

Fig. 6. Primary metabolism analysis of molecules from pneumococci and pharyngeal cells during the acquisition of a pneumococcal ICE. The bioreactor was inoculated with D39 (SPJV22) and GA16833 or D39Δ*comD* and GA16833, and incubated at 37°C. Supernatants coming off the bioreactor chamber were collected for 60 min between 1 and 2 h, or 3 and 4 h, post inoculation. Primary metabolism analysis was performed using sterilized supernatants. (A) PCA biplot of the first two components extracted from a principal components analysis; group membership is indicted, and normal data ellipses for each group. (B) Biplots of the first two components extracted from a partial least squares discriminant analysis, group membership is indicated, and normal data ellipses for each group is shown. (C) Heatmap for the identified compounds. Each column is a pairwise comparison between two groups. Each row is a chemical compound. Asterisks indicate statistical significance from the Mann Whitney U test. The color bar on the side indicates the chemical superclass from the class column. (D) STRING protein interaction network analysis of Nicotinate phosphoribosyltransferase (Spr1733). Shown are 25 edges (interactions) linking 11 proteins (nodes). The average local clustering coefficient was 0.858 and protein-protein interaction enrichment *p* value was 2.24×10^{-4} demonstrating a potential biological interaction among proteins.

TIGR4$^{\Omega ermB}$ and we confirmed that TIGR4Δ*comCDE*$^{\Omega ermB}$ had a significant transformation defect compared with the parent strain (not shown). This new TIGR4Δ*comCDE*$^{\Omega ermB}$ capsule donor strain was incubated along with the recipient D39$^{\text{Str-Tmp}}$ in the bioreactor and transformants with the genotype D39$^{\text{Str-Tmp/Ery}}$ were harvested. The adjusted rF for the acquisition of the capsule locus from TIGR4Δ*comCDE*$^{\Omega ermB}$ into strain D39$^{\text{Str-Tmp}}$ was again significantly different than that of the acquisition of *ermB* (not shown).

Taken together, we demonstrated that the rF for acquiring Mega Class IV(c)/ICE region (~53 kb) by recipient D39$^{\text{Str-Tmp}}$ was three orders of magnitude higher than that to acquire by transformation a homologous *ermB-cps4* locus, indicating the acquisition of ICE may require additional elements other than the transformation machinery.

3. Discussion

Selection of microbes by the acquisition of new genetic traits occurs in complex microbe-host microenvironments. Here, we investigated ultrastructural, metabolic and genetic characteristics occurring during the acquisition of macrolide resistance by pneumococcal strains. *Spn* strains form highly dynamic nasopharyngeal biofilm consortia, with pneumococci fused into "islets". These islets span extracellular and intracellular compartments, where pneumococci are encapsulated, or lacking capsule. We thus propose that transformation occurs in both the extracellular and intracellular compartments. Supporting this hypothesis, recent studies by Echlin and colleagues (2023) successfully transferred antibiotic-resistant genes among pneumococcal strains co-infected in the lungs using a mouse model of invasive pneumococcal infection (Echlin et al., 2023). Relevant to the acquisition of macrolide resistance, the close proximity of bacteria within the islets facilitated rapid acquisition of Mega regardless it was associated with an ICE. We also demonstrated that transformable pneumococci act synergistically with human pharyngeal cells to modify the local metabolic microenvironment to increase the frequency of acquisition of macrolide resistance determinants.

Mega, whether associated with an ICE or not, was transferred at a high frequency in the bioreactor without selective pressure. Moreover, supplementing the bioreactor with sub-MIC erythromycin did not significantly alter the rF for the acquisition of Tn*2009* by *Spn*. In other organisms, selective pressure did not influence the frequency. For example, plasmid transfer frequency of the conjugation plasmid encoding the tetracycline-efflux pump TetA, in *Escherichia coli*, remains unchanged despite the presence of tetracycline (Nolivos et al., 2019; Lopatkin et al., 2016).

Acquisition of genes in the nasopharynx by recombination via transformation has driven the spread of drug resistance, including resistance to beta-lactam antibiotics, and the acquisition of capsule genes in *Spn* strains (Chewapreecha et al., 2014; Scherer et al., 2021). Current methods, however, for studying the rF for the acquisition of large genetic elements carrying antibiotic resistant genes skew the analysis of frequencies toward the antibiotic selection utilized. Experiments in the current study supported this hypothesis by PCR mapping of hundreds of transformants that acquired macrolide resistance carried either upstream of the capsule locus (~28 kb), or Mega Class IV(c) (~53 kb). To our surprise, the adjusted rF for the acquisition of the full-length Mega Class IV(c) insertion was three orders of magnitude higher than that for acquiring the capsule locus. Detailed molecular analysis revealed that >50 % of D39$^{\text{MegaIV(c)}}$ transformants acquired the full-length Mega Class IV(c) insertion region, whereas 11 % transformants screened acquired the full-length capsule locus. Accordingly, our genomics analysis of macrolide-resistant pneumococcal strains isolated in China, identified hot spots of recombination within the ICE's conjugation machinery and the locus encoding for proteins of the transformation apparatus. Elegant *in vitro* transformation studies

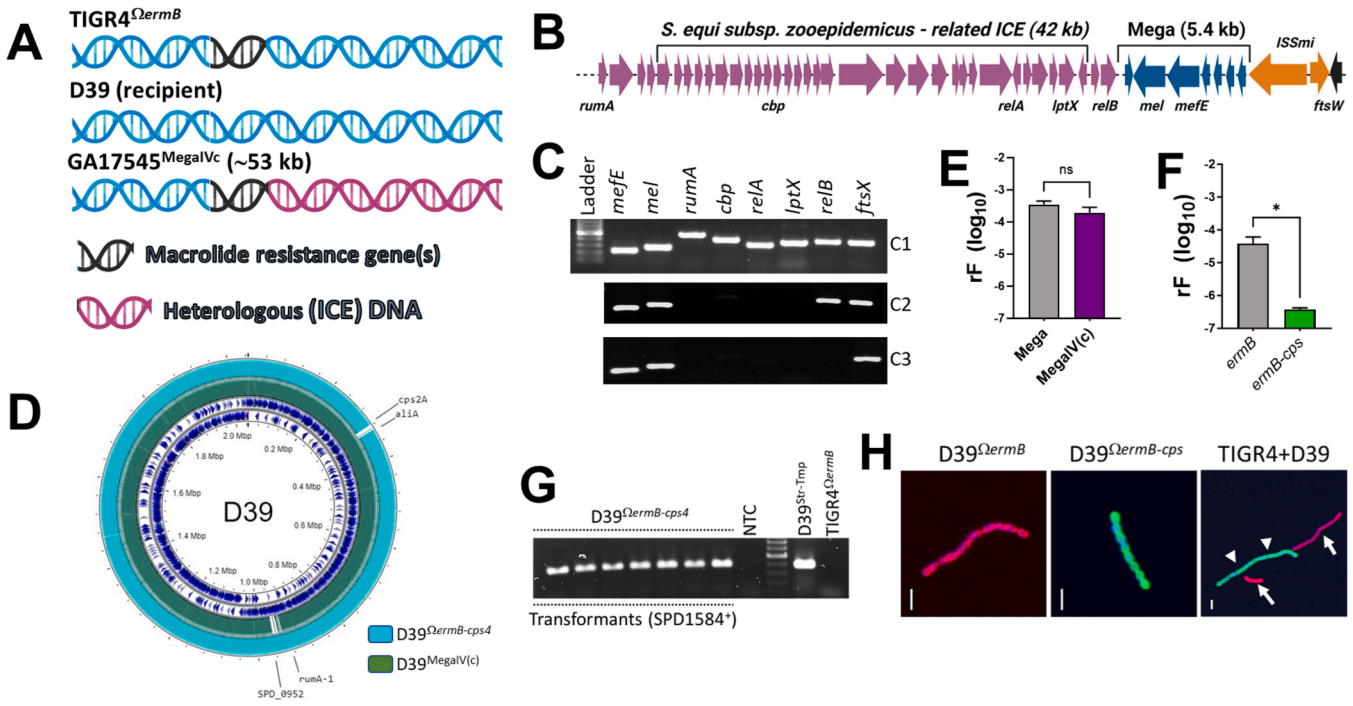

Fig. 7. Recombination frequency for the acquisition of MegaIV(c) or the capsule locus by recipient D39. (A) Diagram representing homologs (blue) and heterologous (red) DNA regions where macrolide resistance genes (black), *ermB* or *mefE/mel* are carried in donor strains TIGR4$^{\Omega ermB}$, or GA17545, as compared to the recipient D39. (B) Schematic map of the ICE including MegaIV(c) from GA17545. Genes utilized as targets in PCR are shown underneath. (C) DNA was extracted from transformants D39$^{MegaIV(c)}$ and utilized as template in PCR reactions. Amplifying genes were shown. (D) Mapping of D39$^{MegaIV(c)}$ and D39 $^{\Omega ermB\ -cps4}$ against recipient D39. (E) D39 (SPJV33) and GA17545 were inoculated in the bioreactor and incubated for 6 h. Biofilm bacteria were harvested from the bioreactor, diluted and platted onto blood agar plates containing the appropriate antibiotics to investigate the recombination frequency (rF). (E) The rF of all transformants (D39$^{MegaIV(c)}$) growing on BAP containing streptomycin, trimethoprim and erythromycin was shown as (Mega). Those D39$^{MegaIV(c)}$ carrying the full-length Mega, as confirmed by PCR, were utilized to adjust the rF and was shown as [MegaIV(c)]. (F) D39 (SPJV33) and TIGR4$^{\Omega ermB}$ were inoculated in the bioreactor and incubated for 6 h. Biofilm bacteria were harvested from the bioreactor, diluted and platted onto blood agar plates (BAP) containing the appropriate antibiotics to investigate the recombination frequency (rF). The rF of all transformants (D39$^{\Omega ermB}$) growing on BAP containing streptomycin, trimethoprim and erythromycin was shown as (*ermB*). Those D39 $^{\Omega ermB}$ carrying the capsule locus from TIGR4, were utilized to adjust the rF and that was shown as (*ermB-cps*). (G) D39 $^{\Omega ermB\ -cps4}$ transformants were DNA extracted and this DNA was used as a template in PCR reactions amplifying the D39 gene SPD_1584, encoding a putative ABC transporter, permease protein. (H) D39$^{\Omega ermB}$, D39 $^{\Omega ermB\ -cps4}$ or a mixture of D39 and TIGR4$^{\Omega ermB}$ was stained with an anti-S2 antibody labeled with Alexa555, and an anti-S4 antibody labeled with Alexa488. Preparations were analyzed by confocal microscopy. Arrows= D39, arrowheads= TIGR4$^{\Omega ermB}$. In all panels Bar=3.

demonstrated that the single largest recombination event in *Spn* resulted in the acquisition of DNA fragments of 30 kb (Cowley et al., 2018). Therefore, acquisition of the entire Mega Class IV(c) insertion (~53 kb) at such different rF, compared with the acquisition of transformation-driven capsule locus, may suggest that additional elements are involved. Recent evidence showing that the acquisition of a ~60 kb SCC*mec* cassette driving the spread of methicillin resistance in *S. aureus* supports the above hypothesis. Acquisition of SCC*mec* was shown to occurs through transformation but it required additional elements including the CcrAB-mediated excision/integration system encoded within SCC*mec* (Maree et al., 2022).

We recently provided evidence that the transformation machinery facilitates the transfer of large ICEs in *Spn* (Antezana et al., 2023). Spontaneous natural competence develops in the bioreactor, facilitating the acquisition of ICEs at a high frequency (~10^{-4}) and indicating that all elements necessary for the transfer of ICEs are present. The absence of human pharyngeal cells, for instance, causes a reduced rF of ~10^{-7} (not shown and (Lattar et al., 2018)). Thus, an orchestrated machinery driven the spread of macrolide resistance involves both bacterial and host cell factors. We have at least two hypotheses to explain why the competence system facilitates these acquisition events. In the first one, we suggest that the competence regulon affects the formation of the DNA exchange islets on human cells, or the proximity of pneumococci within the biofilms. In support to this, competence development has been associated to early events during the attachment of *Spn* to host cells (Vidal et al., 2013; Marks et al., 2012). Whereas the density of *com* mutants was similar as that of the wild type strains in dual strain biofilms (Antezana et al., 2023), early events required for the acquisition ICEs may have been perturbed.

A second hypothesis relates to the metabolite host response against a functional competence system. This can involve the production or absence of a metabolite(s) required to trigger the acquisition of an ICE. For instance, antibiotic-induced changes of metabolites during infection have been recently discovered and the presence of those metabolites affect antibiotic efficacy (Yang et al., 2017). We report here a signature of metabolites depleted at the time of the acquisition of a pneumococcal ICE. These molecules represent novel targets for future interventions to reduce the mobilization of large genetic elements into new hosts.

4. Materials and methods

4.1. Bacterial strains, culture media, and antibiotics

A total of 128 pneumococcal strains isolated from pneumococcal disease cases in China from a previous study (Wu et al., 2022) (Supplementary Table S4), and that were resistant to erythromycin (127 MIC≥128 μg/ml, 1 MIC=4 μg/ml) were whole genome sequenced. Pneumococcal strains used for antibiotic resistance transfer experiments were listed in Supplementary Table S1. Strains were routinely cultured on blood agar plates (BAP), or grown in Todd Hewitt broth containing 0.5 % (w/v) yeast extract (THY), at 37°C with a 5 % CO_2 atmosphere. Where indicated, streptomycin (200 μg/ml), trimethoprim (10 μg/ml),

tetracycline (1 μg/ml), and/or erythromycin (1 μg/ml) was added to BAP. All antibiotics were purchased from Sigma. Bacterial inoculum for all experiments was prepared as previously described (Vidal et al., 2013).

4.2. DNA Extraction, whole genome sequencing analysis, and ICE analysis

Genomic DNA of all tested pneumococcal isolates was extracted using a DNA mini kit (Qiagen, Valencia, CA, USA) and subjected to whole-genome sequencing (WGS) utilizing the Illumina HiSeq2000™ platform. Qualified and trimmed sequence reads (Accession: PRJNA795524) were mapped to a reference strain 19A-19339 (Accession: CP071917) that also carries Tn*2010* to make single nucleotide polymorphism (SNP) calls using Snippy (v4.4.5) (Snippy, 2020) with default parameters and recombination prediction was then conducted via Gubbins (v2.4.1) (Croucher et al., 2015) using full-length alignment from Snippy with the minimum number of 3 for base substitutions required to identify a recombination event. A quality-controlled paired-end fastq file for each tested strain was assembled by Shovill (v0.9.0) (Shovill, 2020), with a minimal length and coverage of 200 bp and 10x, for all contigs. The assemblies of selected recombinants were used to map against the complete sequence of strain D39 (CP000410) in BRIG 0.95 (Alikhan et al., 2011).

D39-derivative transformants were whole-genome sequenced using the NextSeq500 platform, targeting an average of 20 M reads/sample (50X coverage) for the captured samples. The raw Illumina sequence reads were quality-tested by FastQC (v0.12.0) and trimmed by Trim Galore (v0.6.9). Paired-end FastQC files were assembled using SPAdes (v3.11.1). The assembled capsule switch strain was annotated onto the closed genome sequence of the reference strain D39 (CP000410) and $D39^{Tn17545}$ against GA17545 (AFGA01000000) using the online web-based RAPT and Genome Assembly Service tools. Annotated whole-genome sequences have been deposited in NCBI GenBank under BioProject no. PRJNA1055520.

BLASTn (v2.15.0) was used to identify ICEs in all tested strain assemblies by comparison to a database of all known *Spn* ICE sequences. The BLASTn algorithm is particularly effective in identifying homologous sequences within a prepared ICE database. It searches for regions of local similarity between sequences. By aligning the query sequences (in this case, the assembled strain genomes) against the reference database of ICEs, the program identified matches that suggest the presence of ICEs in the test strains. ICEs containing only the *ermB* gene were classified as Tn*6002*-related, while those containing both the Mega element and the *ermB* gene were classified as Tn*2010*-related.

4.3. Cell cultures

Human pharyngeal Detroit 562 cells (ATCC CCL-138) were cultured in Gibco™ Minimum Essential Media (MEM) (Thermo Fisher Scientific, Waltham, MA) supplemented with 10 % non-heat-inactivated fetal bovine serum (FBS) (Atlanta biologicals), 1 % nonessential amino acids (Sigma), 1 % glutamine (Sigma), penicillin (10,000 U/ml)-streptomycin (10,000 μg/ml), and HEPES (10 mM) (Gibco). For the seeding, cells were harvested with 0.25 % trypsin (Gibco), resuspended in the cell culture medium at a ratio of 1:5 and incubated at 37°C in a 5 % CO_2 humidified atmosphere.

4.4. Bioreactor system

Detroit 562 cells were grown on Snapwell™ filters (Corning, USA) and placed in a sterile vertical diffusion chamber (i.e., bioreactor) (Vidal et al., 2013). Bioreactor chambers were perfused as detailed in our previous publication (Lattar et al., 2018). Chambers were inoculated with ~$1x10^8$ cfu/ml of each pneumococcal strain and incubated at ~34°C under a sterile environment. At the end of the incubation, Snapwell inserts were removed and pneumococci were harvested by sonication for 15 s in a Bransonic ultrasonic water bath (Branson, Danbury, CT), followed by extensive pipetting to remove attached bacteria. An aliquot was used to obtain the density of each strain, by serial dilution and platting on BAP containing the appropriate antibiotic, and another aliquot was plated onto BAP containing two, or three antibiotics, to harvest recombinants.

4.5. Analysis of nasopharyngeal pneumococcal biofilm consortia by confocal microscopy

To visualize pneumococci by super-resolution and confocal microscopy, we installed a glass coverslip inside the Snapwell™ filters prior to seeding human pharyngeal cells. Once pharyngeal cells became polarized, the Snapwell was installed in the bioreactor and inoculated as above. At the end of the incubation, the coverslip containing pharyngeal cells with pneumococcal biofilms were washed twice with PBS and fixed with 2 % PFA for 15 min at room temperature. Biofilms were then washed with PBS and blocked with 2 % bovine serum albumin (BSA) for 1 h at room temperature. The cells containing biofilms were simultaneously incubated with serotype-specific polyclonal antibodies (Statens Serum Institute, Denmark) (~ 40 μg/ml), and wheat germ agglutinin (WGA) conjugated with Alexa Fluor (488 or 555, Invitrogen), for 1 h at room temperature. Antibodies had been previously labeled with Alexa-488 (anti-S4/A488) or Alexa-555 (anti-S2/A555 and anti-S6B/A555) following the manufacturer recommendations (Molecular Probes) (Lattar et al., 2018; Wu et al., 2017). Stained preparations were finally washed two times with PBS and mounted with ProLong Diamond Antifade agent with DAPI (Molecular Probes). Super-resolution confocal images were obtained using an Olympus FV1000 confocal microscope. Confocal micrographs were analyzed with ImageJ version 1.49k (National Institutes of Health, USA) or with the Imaris software 10.1.0 (Bitplane AG).

4.6. Ultrastructural studies

Electron microscopy was used to visualize the detailed spatial localization of pneumococcal strains within nasopharyngeal biofilm consortia and their interactions. Instead of a glass coverslip as described above, we installed a square chip inside the Snapwell™, or a Thermanox coverslip (Fisher scientific), and then cells were grown and infected as detailed in the previous section. At the end of incubation, the square silicon chip, or Thermanox coverlis, was removed from the bioreactor culture chamber and processed as detailed below. Silicon chips, or Thermanox, were immediately fixed with a 2.5 % glutaraldehyde solution in 0.1 M cacodylate buffer pH 7.4 overnight and then washed with the same buffer. Preparations were processed for scanning electron microscopy (SEM) as follows: post-fixed with 1 % osmium tetroxide and 1.5 % potassium ferrocyanide in 0.1 M cacodylate buffer for one hour. They were subsequently rinsed with de-ionized water, followed by dehydration through an ethanol series ending with three exchanges of absolute ethanol. The samples were then placed into individual ventilated processing vessels in fresh absolute ethanol and placed into a Polaron E3000 critical point drying unit where the ethanol was exchanged for liquid CO_2. This liquid CO_2 was eventually brought to its critical point of 1073 psi at 31°C and allowed to slowly vent. Dried samples were then secured to labeled aluminum SEM stubs and coated with approximately 15 nm of chromium with a Denton DV-602 Turbo Magnetron Sputter coater. Samples were then viewed with a Topcon DS130F field emission scanning electron microscope using 5 kV accelerating voltage. Transmission electron microscopy (TEM). Preparations on Thermanox were infiltrated and embedded in Eponate 12 resin. Ultrathin sections were cut on a RMC PowerTome XL ultramicrotome at 70 nm, stained with 5 % aqueous uranyl acetate and 2 % lead citrate, and examined on a JEOL IEM-1400 transmission electron microscope equipped with Gatan UltraScan US1000.894 and Orius SC1000.832 CCD

cameras.

4.7. PCR studies of transformants

Endpoint qPCR and conventional PCR reactions of transformants were conducted for genotypical confirmation. Quantitative PCR reactions targeting serotype 2 or serotype 4 were performed to identified D39$^{Str/Tmp}$ transformants that acquired *ermB*-cpsTIGR4. Primer and probe of these serotype-specific qPCR reactions (Sakai et al., 2015) are listed in Supplementary Table S3. qPCR reactions were performed with 2x PerfeCTa qPCR ToughMix, 300 nM of each primer and 200 nM 6FAM-BHQ1 probe. Reactions were run using a CFX96 Real-Time PCR Detection System (Bio-Rad) with the following conditions: 1 cycle at 50°C for 2 minutes, 1 cycle at 95°C for 2 minutes, 40 cycles of 95°C for 15 seconds, and 1 cycle of 60°C for 1 minute.

Transformants identified by qPCR to carry serotype 4 capsule genes were propagated on BAP with erythromycin and the DNA was extracted. This DNA was utilized as template in conventional PCR reactions with primers that amplify either the *ermB* gene, serotype 4 capsule genes, or primers JVS0415/JVS0416 that amplify D39-specific SPD_1584 gene (Supplementary Table S3). PCR reactions were performed using MegaFi Fidelity 2x PCR MasterMix, 1 μM of each primer, and nuclease free water and run in a C1000 Touch™ Thermal Cycler (Bio-Rad).

PCR reactions utilized to screen acquisition of Tn2009 by D39 $^{Str/Tmp}$ used primer pairs F1 through F6 (Supplementary Table S3). Conventional PCR reactions were performed to identify D39$^{Str/Tmp}$ transformants that had acquired the full-length Mega Class IV(c) region. D39^{MegaIVc} transformants were patched onto BAP plates containing streptomycin, trimethoprim and erythromycin. DNA was extracted from patches with Quellex, and used in eight different PCR reactions. The eight-individual primer pairs amplified the following genes or putative genes: *mel* (JVS149/JVS150…224 bp), *mef*(A) (JVS151/JVS152), *rumA* (JVS225/JVS226), a gene encoding a conjugative transposon cell wall hydrolase (JVS227/JVS228), gene encoding a putative relaxase/mobilization nuclease domain protein (JVS229/JVS230), a gene encoding a putative LPXTG-motif cell wall anchor domain protein (JVS231/JVS232), a gene encoding a site-specific recombinase/resolvase family protein (JVS233/JVS234), and *ftsW* (JVS235/JVS236).

4.8. DNA Extraction and serotype-specific qPCR reactions

DNA was extracted from 200 μl of a fresh suspension of pneumococcal strains or a pool of recovered recombinants with the QIAamp DNA Mini kit according to the manufacturer's instructions. Final elution was done with 100 μl of elution buffer, DNA preps were quantified using a Nanodrop™2000 spectrophotometer (Thermo Fisher, Wilmington, Delaware, USA). DNA preps were utilized as templates for serotype-specific quantitative PCR reactions with primers and probes listed in Supplementary Table S3 to identify the serotype of each strain as well as recombinants as detailed in our previous studies (Lattar et al., 2018; Sakai et al., 2015, 2017).

4.9. Insertion of ermB near the capsule locus of strain TIGR4

The *ermB* gene was PCR amplified using DNA template from SPJV10[13] and primers Ery-L-*Xba*I and Ery-R-*Xho*I listed in a previous publication (Vidal et al., 2013). This *ermB* PCR product was purified using the QIAquick PCR Purification Kit (Qiagen, Valencia CA) and then digested with restriction enzyme *Xba*I. Simultaneously two ~1.5 kb PCR products, to be cloned flanking *ermB,* were PCR amplified using DNA from strain TIGR4 as a template and primers JVS95L and JVS96R, to generate an upstream fragment, or JVS97L and JVS98R to generate a downstream fragment. PCR products were purified as above and digested with *Xba*I (upstream) or *Xho*I (downstream). The *Xba*I-digested upstream fragment was first ligated using T4 DNA ligase and the ligated product was used as a template in PCR reactions using primers JVS95L and Ery-R-*Xho*I. This purified PCR product was digested with *Xho*I and ligated to the *Xho*I-digested downstream fragment as mentioned. The final ligated fragment was used as a template in PCR reactions with primers JVS95L and JVS98R, purified as indicated above and sequenced at Eurofins to confirm the construct. This cassette containing sequences downstream the capsule locus was transformed (~100 ng) into competent cells of strain TIGR4 wt. A transformant recovered in BAP with erythromycin (1 μg/ml), named SPJV24, was serotyped with Quellung antisera (Statens Serum Institute, Copenhagen, Denmark) to confirm expression of serotype 4 capsule, and then DNA extracted to confirm the *ermB* was located upstream the capsule locus, as detailed in the Results section.

4.10. Construction of a TIGR4$^{\Omega ermB}$ΔcomCDE mutant

The mutation was prepared by replacing the operon *comCDE* in TIGR4$^{\Omega ermB}$ with a truncated fragment containing the *catP* gene. This fragment was amplified from a GA16833Δ*comCDE* mutant (SPJV37) by PCR with primers JVS0413 and JVS0414 (Supplementary Table S3). The mutants were selected on BAP containing chloramphenicol (3 μg/ml). The mutation was confirmed by PCR in the resulting chloramphenicol-resistant clones.

4.11. Primary metabolism analysis of mixtures of S. pneumoniae strains infecting human pharyngeal cells

D39 and GA16833 or D39Δ*comD* and GA16833, were infected into the bioreactor as previous detailed, and infected cells were incubated at 37°C. The influx coming off the bioreactor chamber (i.e., supernatant and planktonic bacteria) was collected for 60 min after the first hour of incubation, or after 3 h of incubation. Supernatants were filter sterilized with a 0.4 μm syringe filter and immediately frozen at −80°C. Primary metabolism by gas chromatography-time of flight mass spectrometry (GC-TOF MS) was performed at the West Coast Metabolomics Center, UC Davis. Briefly, samples were extracted using 1 ml of 3:3:2 ACN:IPA:H_2O (v/v/v). Half of the sample was dried to completeness and then derivatized using 10 μl of 40 mg/ml of methoxyamine in pyridine. They were shaken at 30°C for 1.5 h. Then 91 μl of MSTFA + FAMEs to each sample and they were shaken at 37°C for 0.5 h to finish derivatization. Samples were then vialed, capped, and injected onto the instrument. We use a 7890 A GC coupled with a LECO TOF. 0.5 μl of derivatized sample is injected using a splitless method onto a RESTEK RTX-5SIL MS column with an Intergra-Guard at 275°C with a helium flow of 1 ml/min. The GC oven is set to hold at 50°C for 1 min then ramp to 20 °C/min to 330°C and then hold for 5 min. The transferline was set to 280°C while the EI ion source was set to 250°C. The Mass spec parameters collect data from 85 *m/z* to 500 *m/z* at an acquisition rate of 17 spectra/sec. Raw data were processed by LECO ChromaTOF version 4.5 for baseline subtraction, deconvolution and peak detection, while BinBase was used for annotation and reporting (Skogerson et al., 2011).

4.12. Statistical analysis

We performed one-way analysis of variances (ANOVA) followed by Dunnet's multiple comparison test when more than two groups were compared or Student *t* test to compare two groups, as indicated. All statistical analysis was performed using the software Graph Pad Prism (version 8.3.1).

CRediT authorship contribution statement

Jorge Eugenio Vidal: Writing – review & editing, Writing – original draft, Methodology, Investigation, Funding acquisition, Formal analysis, Conceptualization. **Xi Xiang:** Investigation. **Yunsong Yu:** Writing – review & editing, Funding acquisition, Formal analysis, Conceptualization. **Brenda Antezana:** Writing – review & editing, Investigation.

Austin A Medders: Investigation. **Fuminori Sakai:** Writing – review & editing, Investigation. **Santiago Lattar:** Writing – review & editing, Investigation. **David Ashley Robinson:** Writing – review & editing, Investigation. **Yih-Ling Tzeng:** Writing – review & editing, Investigation, Funding acquisition, Formal analysis, Conceptualization. **Ana Gabriela Jop Vidal:** Investigation, Formal analysis. **Lance Keller:** Writing – review & editing, Investigation. **Babek Alibayov:** Writing – review & editing, Methodology, Investigation, Formal analysis, Conceptualization. **David Stephens:** Writing – review & editing, Investigation, Funding acquisition, Formal analysis, Conceptualization. **Xueqing Wu:** Writing – review & editing, Writing – original draft, Methodology, Investigation, Funding acquisition, Formal analysis, Conceptualization.

Declaration of Competing Interest

The authors declare that they have no known competing financial interests or personal relationships that could have appeared to influence the work reported in this paper.

Acknowledgments

This study was primarily supported by the National Institutes of Health (NIH; R21AI112768-01A1, 7R21AI144571-02, and 1R01AI175461-01A1), the Natural Science Foundation of Zhejiang Province (LY24H190003), and the National Natural Science Foundation of China (No. 32000092) to XW, and the Jinhua Science and Technology Research Key program (No. 2021-3-07) to XX. JEV is also supported by a grant from NIGMS through the Molecular Center of Health and Disease (1P20GM144041–01A1 7651). The work performed through the UMMC Molecular and Genomics Facility is supported, in part, by funds from the NIGMS, including the Mississippi INBRE (P20GM103476) and Obesity, Cardiorenal and Metabolic Diseases-COBRE (P30GM149404). Special thanks to Dr. Lesley McGee and Dr. Bernard Beall from the Centers for Disease Control and Prevention (CDC) for providing pneumococcal invasive isolates, and to Dr Shanshan Zhao for provide clinical multidrug resistant pneumococci. We thank Dr. Hong Yi, and Dr. Jeannette Taylor for their assistance with electron microscopy at the Robert P. Apkarian Integrated Electron Microscopy Core in Emory University. Authors appreciate the assistance of Dr. Neil Anthony, from Emory University School of Medicine, with confocal microscopy, and Dr. Veronique Parrot for her assistance on preparing some figures.

Appendix A. Supporting information

Supplementary data associated with this article can be found in the online version at doi:10.1016/j.drup.2024.101138.

References

Aliberti, S., Cook, G.S., Babu, B.L., Reyes, L.F., Sanz, A.H.R., Soni, F., Anzueto, N.J., Faverio, A., Sadud, P., Muhammad, R.F., Prat, I., Vendrell, C., Neves, E., Kaimakamis, J., Feneley, E., Swarnakar, A., Franzetti, R., Carugati, F., Morosi, M., Monge, M., Restrepo, E., investigators G, M.I., 2019. International prevalence and risk factors evaluation for drug-resistant *Streptococcus pneumoniae* pneumonia. Epub 2019/07/13. J. Infect. https://doi.org/10.1016/j.jinf.2019.07.004.

Alikhan, N.F., Petty, N.K., Ben Zakour, N.L., Beatson, S.A., 2011. BLAST Ring Image Generator (BRIG): simple prokaryote genome comparisons. Epub 20110808. BMC Genom. 12, 402. https://doi.org/10.1186/1471-2164-12-402.

Antezana, B.S., Lohsen, S., Wu, X., Vidal, J.E., Tzeng, Y.L., Stephens, D.S., 2023. Dissemination of Tn916-related integrative and conjugative elements in *Streptococcus pneumoniae* occurs by transformation and homologous recombination in Nasopharyngeal Biofilms. e0375922. Epub 20230313 Microbiol. Spectr. 11 (2). https://doi.org/10.1128/spectrum.03759-22.

Azarian, T., Mitchell, P.K., Georgieva, M., Thompson, C.M., Ghouila, A., Pollard, A.J., von Gottberg, A., du Plessis, M., Antonio, M., Kwambana-Adams, B.A., Clarke, S.C., Everett, D., Cornick, J., Sadowy, E., Hryniewicz, W., Skoczynska, A., Moisi, J.C., McGee, L., Beall, B., Metcalf, B.J., Breiman, R.F., Ho, P.L., Reid, R., O'Brien, K.L., Gladstone, R.A., Bentley, S.D., Hanage, W.P., 2018. Global emergence and population dynamics of divergent serotype 3 CC180 pneumococci. Epub 20181126. PLoS Pathog. 14 (11), e1007438 https://doi.org/10.1371/journal.ppat.1007438.

Chaguza, C., Senghore, M., Bojang, E., Gladstone, R.A., Lo, S.W., Tientcheu, P.E., Bancroft, R.E., Worwui, A., Foster-Nyarko, E., Ceesay, F., Okoi, C., McGee, L., Klugman, K.P., Breiman, R.F., Barer, M.R., Adegbola, R.A., Antonio, M., Bentley, S. D., Kwambana-Adams, B.A., 2020. Within-host microevolution of *Streptococcus pneumoniae* is rapid and adaptive during natural colonisation. Epub 20200710. Nat. Commun. 11 (1), 3442. https://doi.org/10.1038/s41467-020-17327-w.

Chancey, S.T., Agrawal, S., Schroeder, M.R., Farley, M.M., Tettelin, H., Stephens, D.S., 2015. Composite mobile genetic elements disseminating macrolide resistance in *Streptococcus pneumoniae*. Epub 2015/02/25 Front Microbiol 6, 26. https://doi.org/10.3389/fmicb.2015.00026.

Chao, Y., Marks, L.R., Pettigrew, M.M., Hakansson, A.P., 2014. *Streptococcus pneumoniae* biofilm formation and dispersion during colonization and disease. Front Cell Infect. Microbiol. 4, 194. https://doi.org/10.3389/fcimb.2014.00194.

Chewapreecha, C., Harris, S.R., Croucher, N.J., Turner, C., Marttinen, P., Cheng, L., Pessia, A., Aanensen, D.M., Mather, A.E., Page, A.J., Salter, S.J., Harris, D., Nosten, F., Goldblatt, D., Corander, J., Parkhill, J., Turner, P., Bentley, S.D., 2014. Dense genomic sampling identifies highways of pneumococcal recombination. Epub 2014/02/11. Nat. Genet 46 (3), 305–309. https://doi.org/10.1038/ng.2895.

Claverys, J.P., Martin, B., Polard, P., 2009. The genetic transformation machinery: composition, localization, and mechanism. Epub 20090218. FEMS Microbiol Rev. 33 (3), 643–656. https://doi.org/10.1111/j.1574-6976.2009.00164.x.

Cowley, L.A., Petersen, F.C., Junges, R., Jimson, D.J.M., Morrison, D.A., Hanage, W.P., 2018. Evolution via recombination: Cell-to-cell contact facilitates larger recombination events in *Streptococcus pneumoniae*. Epub 2018/06/14. PLoS Genet. 14 (6), e1007410 https://doi.org/10.1371/journal.pgen.1007410.

Croucher, N.J., Chewapreecha, C., Hanage, W.P., Harris, S.R., McGee, L., van der Linden, M., Song, J.H., Ko, K.S., de Lencastre, H., Turner, C., Yang, F., Sa-Leao, R., Beall, B., Klugman, K.P., Parkhill, J., Turner, P., Bentley, S.D., 2014. Evidence for soft selective sweeps in the evolution of pneumococcal multidrug resistance and vaccine escape. Epub 20140610. Genome Biol. Evol. 6 (7), 1589–1602. https://doi.org/10.1093/gbe/evu120.

Croucher, N.J., Page, A.J., Connor, T.R., Delaney, A.J., Keane, J.A., Bentley, S.D., Parkhill, J., Harris, S.R., 2015. Rapid phylogenetic analysis of large samples of recombinant bacterial whole genome sequences using Gubbins. Epub 2014/11/22. Nucleic Acids Res. 43 (3), e15 https://doi.org/10.1093/nar/gku1196.

Del Grosso, M., Camilli, R., Iannelli, F., Pozzi, G., Pantosti, A., 2006. The mef(*E*)-carrying genetic element (mega) of *Streptococcus pneumoniae*: insertion sites and association with other genetic elements. Antimicrob. Agents Chemother. 50 (10), 3361–3366. https://doi.org/10.1128/AAC.00277-06.

Del Grosso, M., Camilli, R., Libisch, B., Fuzi, M., Pantosti, A., 2009. New composite genetic element of the Tn916 family with dual macrolide resistance genes in a *Streptococcus pneumoniae* isolate belonging to clonal complex 271. Epub 20081222. Antimicrob. Agents Chemother. 53 (3), 1293–1294. https://doi.org/10.1128/AAC.01066-08.

Del Grosso, M., Scotto d'Abusco, A., Iannelli, F., Pozzi, G., Pantosti, A., 2004. Tn2009, a Tn916-like element containing mef(E) in *Streptococcus pneumoniae*, 2037-42. Epub 2004/05/25. doi Antimicrob. Agents Chemother. 48 (6). https://doi.org/10.1128/AAC.48.6.2037-2042.2004.

Domenech, A., Ardanuy, C., Grau, I., Calatayud, L., Pallares, R., Fenoll, A., Brueggemann, A.B., Linares, J., 2014. Evolution and genetic diversity of the Spain23F-ST81 clone causing adult invasive pneumococcal disease in Barcelona (1990-2012). Epub 20131208. J. Antimicrob. Chemother. 69 (4), 924–931. https://doi.org/10.1093/jac/dkt473.

Echlin, H., Iverson, A., Sardo, U., Rosch, J.W., 2023. Airway proteolytic control of pneumococcal competence. Epub 20230531. PLoS Pathog. 19 (5), e1011421 https://doi.org/10.1371/journal.ppat.1011421.

French, J.B., Cen, Y., Sauve, A.A., Ealick, S.E., 2010. High-resolution crystal structures of *Streptococcus pneumoniae* nicotinamidase with trapped intermediates provide insights into the catalytic mechanism and inhibition by aldehydes. Epub 20100920. Biochemistry 49 (40), 8803–8812. https://doi.org/10.1021/bi1012436.

Gay, K., Stephens, D.S., 2001. Structure and dissemination of a chromosomal insertion element encoding macrolide efflux in *Streptococcus pneumoniae*. Epub 20010531. J. Infect. Dis. 184 (1), 56–65. https://doi.org/10.1086/321001.

Gilley, R.P., Orihuela, C.J., 2014. Pneumococci in biofilms are non-invasive: implications on nasopharyngeal colonization. Epub 2014/11/22. doi Front Cell Infect. Microbiol. 4, 163. https://doi.org/10.3389/fcimb.2014.00163.

Hall-Stoodley, L., Nistico, L., Sambanthamoorthy, K., Dice, B., Nguyen, D., Mershon, W. J., Johnson, C., Hu, F.Z., Stoodley, P., Ehrlich, G.D., Post, J.C., 2008. Characterization of biofilm matrix, degradation by DNase treatment and evidence of capsule downregulation in *Streptococcus pneumoniae* clinical isolates. BMC Microbiol. 8, 173. https://doi.org/10.1186/1471-2180-8-173.

Johnson, C.M., Grossman, A.D., 2015. Integrative and conjugative elements (ICEs): what they do and how they work. Epub 20151014. Annu Rev. Genet 49, 577–601. https://doi.org/10.1146/annurev-genet-112414-055018.

Kim, L., McGee, L., Tomczyk, S., Beall, B., 2016. Biological and epidemiological features of antibiotic-resistant *Streptococcus pneumoniae* in pre- and post-conjugate vaccine eras: a united states perspective. Clin. Microbiol. Rev. 29 (3), 525–552. https://doi.org/10.1128/CMR.00058-15.

Lan, Y., Liu, L., Hu, D., Ge, L., Xiang, X., Peng, M., Fu, Y., Wang, Y., Li, S., Chen, Y., Jiang, Y., Tu, Y., Vidal, J.E., Yu, Y., Chen, Z., Wu, X., 2023. Limited protection of pneumococcal vaccines against emergent *Streptococcus pneumoniae* serotype 14/ST876 strains. Epub 20231102. Infection https://doi.org/10.1007/s15010-023-02110-y.

Lattar, S.M., Wu, X., Brophy, J., Sakai, F., Klugman, K.P., Vidal, J.E., 2018. A mechanism of unidirectional transformation, leading to antibiotic resistance, occurs within

Nasopharyngeal Pneumococcal Biofilm Consortia. MBio 9 (3). https://doi.org/10.1128/mBio.00561-18.
Leclercq, R., Courvalin, P., 2002. Resistance to macrolides and related antibiotics in *Streptococcus pneumoniae*. Antimicrob. Agents Chemother. 46 (9), 2727–2734. https://doi.org/10.1128/AAC.46.9.2727-2734.2002.
Lopatkin, A.J., Huang, S., Smith, R.P., Srimani, J.K., Sysoeva, T.A., Bewick, S., Karig, D. K., You, L., 2016. Antibiotics as a selective driver for conjugation dynamics. Epub 20160411. Nat. Microbiol 1 (6), 16044 https://doi.org/10.1038/nmicrobiol.2016.44.
Malisova, L., Urbaskova, P., Jakubu, V., Spanelova, P., Kozakova, J., Musilek, M., Zemlickova, H., 2019. Surveillance of antibiotic resistance of *Streptococcus pneumoniae* in the Czech Republic, respiratory study results, 2010-2017. Epidemiol. Mikrobiol. Imunol. 68 (2), 75–81.
Maree, M., Thi Nguyen, L.T., Ohniwa, R.L., Higashide, M., Msadek, T., Morikawa, K., 2022. Natural transformation allows transfer of SCCmec-mediated methicillin resistance in *Staphylococcus aureus* biofilms. Epub 20220505. Nat. Commun. 13 (1), 2477. https://doi.org/10.1038/s41467-022-29877-2.
Marks, L.R., Parameswaran, G.I., Hakansson, A.P., 2012. Pneumococcal interactions with epithelial cells are crucial for optimal biofilm formation and colonization in vitro and in vivo. Epub 2012/05/31. Infect. Immun. 80 (8), 2744–2760. https://doi.org/10.1128/IAI.00488-12.
McDougal, L.K., Tenover, F.C., Lee, L.N., Rasheed, J.K., Patterson, J.E., Jorgensen, J.H., LeBlanc, D.J., 1998. Detection of Tn917-like sequences within a Tn916-like conjugative transposon (Tn3872) in erythromycin-resistant isolates of *Streptococcus pneumoniae*. Antimicrob. Agents Chemother. 42 (9), 2312–2318. https://doi.org/10.1128/AAC.42.9.2312.
Nikolaou, E., Hubbard, A.T.M., Botelho, J., Marschall, T.A.M., Ferreira, D.M., Roberts, A. P., 2020. Antibiotic resistance is associated with integrative and conjugative elements and genomic islands in naturally circulating *Streptococcus pneumoniae* Isolates from adults in Liverpool, UK. Epub 20200606. Genes (Basel) 11 (6) https://doi.org/10.3390/genes11060625.
Nolivos, S., Cayron, J., Dedieu, A., Page, A., Delolme, F., Lesterlin, C., 2019. Role of AcrAB-TolC multidrug efflux pump in drug-resistance acquisition by plasmid transfer. Science 364 (6442), 778–782. https://doi.org/10.1126/science.aav6390.
Pimenta, F.C., Roundtree, A., Soysal, A., Bakir, M., du Plessis, M., Wolter, N., von Gottberg, A., McGee, L., Carvalho Mda, G., Beall, B., 2013. Sequential triplex real-time PCR assay for detecting 21 pneumococcal capsular serotypes that account for a high global disease burden. Epub 2012/12/12. J. Clin. Microbiol. 51 (2), 647–652. https://doi.org/10.1128/JCM.02927-12.
Rodgers, G.L., Klugman, K.P., 2011. The future of pneumococcal disease prevention. Epub 2011/09/16. Vaccine 29 (Suppl 3), C43–C48. https://doi.org/10.1016/j.vaccine.2011.07.047.
Sakai, F., Chochua, S., Satzke, C., Dunne, E.M., Mulholland, K., Klugman, K.P., Vidal, J. E., 2015. Single-plex quantitative assays for the detection and quantification of most pneumococcal serotypes. PLoS One 10 (3), e0121064. https://doi.org/10.1371/journal.pone.0121064. PubMed PMID: 25798884; PMCID: PMC4370668.
Sakai, F., Sonaty, G., Watson, D., Klugman, K.P., Vidal, J.E., 2017. Development and characterization of a synthetic DNA, NUversa, to be used as a standard in quantitative polymerase chain reactions for molecular pneumococcal serotyping. FEMS Microbiol. Lett. 364 (17) https://doi.org/10.1093/femsle/fnx173.
Santoro, F., Vianna, M.E., Roberts, A.P., 2014. Variation on a theme; an overview of the Tn916/Tn1545 family of mobile genetic elements in the oral and nasopharyngeal streptococci. Epub 20141020 Front Microbiol 5, 535. https://doi.org/10.3389/fmicb.2014.00535.
Scherer, E.M., Beall, B., Metcalf, B., 2021. Serotype-switch variant of multidrug-resistant *Streptococcus pneumoniae* sequence type 271. Epub 2021/04/30. Emerg. Infect. Dis. 27 (6), 1689–1692. https://doi.org/10.3201/eid2706.203629.
Schroeder, M.R., Lohsen, S., Chancey, S.T., Stephens, D.S., 2019. High-level macrolide resistance due to the mega element [mef(E)/mel] in *Streptococcus pneumoniae*. Epub 2019/05/21. Front Microbiol. 10, 868. https://doi.org/10.3389/fmicb.2019.00868.
Shak, J.R., Vidal, J.E., Klugman, K.P., 2013. Influence of bacterial interactions on pneumococcal colonization of the nasopharynx. Epub 2013/01/01. Trends Microbiol. 21 (3), 129–135. https://doi.org/10.1016/j.tim.2012.11.005.
Shinohara, K., Fujisawa, T., Chang, B., Ito, Y., Suga, S., Matsumura, Y., Yamamoto, M., Nagao, M., Ohnishi, M., Sugai, M., Nakano, S., 2023. Frequent transmission of *Streptococcus pneumoniae* Serotype 35B and 35D, clonal complex 558 Lineage, across continents and the formation of multiple clades in Japan. Epub 20230118 Antimicrob. Agents Chemother. 67 (2), e0108322. https://doi.org/10.1128/aac.01083-22.
Shovill [cited 2020 December 2]. Available from: ⟨https://github.com/tseemann/shovill⟩.
Simell, B., Auranen, K., Kayhty, H., Goldblatt, D., Dagan, R., O'Brien, K.L., 2012. The fundamental link between pneumococcal carriage and disease. Epub 2012/08/24 Expert Rev. Vaccin. 11 (7), 841–855. https://doi.org/10.1586/erv.12.53.
Skogerson, K., Wohlgemuth, G., Barupal, D.K., Fiehn, O., 2011. The volatile compound BinBase mass spectral database. Epub 20110804. BMC Bioinforma. 12, 321. https://doi.org/10.1186/1471-2105-12-321.
Snippy [cited 2020 December 1]. Available from: ⟨https://github.com/tseemann/snippy⟩.
Vidal, A.G.J., Alibayov, B., Frame, I.J., Murin, L., Creel, A., Hu, D., Wu, X., Vidal, J.E., 2022. Induction of the macrolide-resistance efflux pump Mega inhibits intoxication of *Staphylococcus aureus* strains by *Streptococcus pneumoniae*. Epub 20220716. Microbiol. Res. 263, 127134 https://doi.org/10.1016/j.micres.2022.127134.
Vidal, J.E., Howery, K.E., Ludewick, H.P., Nava, P., Klugman, K.P., 2013. Quorum-sensing systems LuxS/autoinducer 2 and Com regulate *Streptococcus pneumoniae* biofilms in a bioreactor with living cultures of human respiratory cells. Infect. Immun. 81 (4), 1341–1353. https://doi.org/10.1128/IAI.01096-12.
Vidal, J.E., Ludewick, H.P., Kunkel, R.M., Zahner, D., Klugman, K.P., 2011. The LuxS-dependent quorum-sensing system regulates early biofilm formation by *Streptococcus pneumoniae* strain D39. Infect. Immun. 79 (10), 4050–4060. https://doi.org/10.1128/IAI.05186-11.
Watson, D.A., Musher, D.M., 1990. Interruption of capsule production in *Streptococcus pneumoniae* serotype 3 by insertion of transposon Tn916. Infect. Immun. 58 (9), 3135–3138. https://doi.org/10.1128/iai.58.9.3135-3138.1990.
Weiser, J.N., 2010. The pneumococcus: why a commensal misbehaves. Epub 2009/11/10. J. Mol. Med. (Berl.) 88 (2), 97–102. https://doi.org/10.1007/s00109-009-0557-x.
Wu, X., Jacobs, N.T., Bozio, C., Palm, P., Lattar, S.M., Hanke, C.R., Watson, D.M., Sakai, F., Levin, B.R., Klugman, K.P., Vidal, J.E., 2017. Competitive dominance within biofilm consortia regulates the relative distribution of Pneumococcal nasopharyngeal density. Appl. Environ. Microbiol. 83 (16) https://doi.org/10.1128/AEM.00953-17.
Wu, X., Zhao, S., Jiang, Y., Xiang, X., Ge, L., Chen, Q., Wang, Y., Vidal, J.E., Yu, Y., 2022. Effect of pneumococcal conjugate vaccine availability on *Streptococcus pneumoniae* infections and genetic recombination in Zhejiang, China from 2009 to 2019. Emerg. Microbes Infect. 11 (1), 606–615. https://doi.org/10.1080/22221751.2022.2040921.
Wyres, K.L., van Tonder, A., Lambertsen, L.M., Hakenbeck, R., Parkhill, J., Bentley, S.D., Brueggemann, A.B., 2013. Evidence of antimicrobial resistance-conferring genetic elements among pneumococci isolated prior to 1974. Epub 20130724. BMC Genom. 14, 500. https://doi.org/10.1186/1471-2164-14-500.
Yang, J.H., Bhargava, P., McCloskey, D., Mao, N., Palsson, B.O., Collins, J.J., 2017. Antibiotic-induced changes to the host metabolic environment inhibit drug efficacy and alter immune function. e3. Epub 20171130 Cell Host Microbe 22 (6), 757–765. https://doi.org/10.1016/j.chom.2017.10.020.